

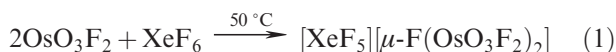
polar-covalent fluorides is diminished relative to that of gas-phase OsO_3F_2 because the fluoride ion donor must be sufficiently fluoro-basic to disrupt the $\text{Os}\cdots\text{F}\cdots\text{Os}$ bridge bonds of the polymeric solid-state structure of $(\text{OsO}_3\text{F}_2)_\infty$.¹²

In contrast, XeF_6 is the strongest fluoride ion donor among the binary fluorides of xenon,¹³ and forms a large number of XeF_5^+ and $\text{Xe}_2\text{F}_{11}^+$ salts with a variety of Lewis acid fluorides having a wide range of fluoride ion acceptor strengths (see Supporting Information for a comprehensive list of known XeF_5^+ and $\text{Xe}_2\text{F}_{11}^+$ salts and their references). The XeF_5^+ and $\text{Xe}_2\text{F}_{11}^+$ cations are extensively associated with their anions through fluorine bridge contacts. In the present study, the reactivity of $(\text{OsO}_3\text{F}_2)_\infty$ with the moderately strong fluoride ion donor, XeF_6 , is investigated. The syntheses and characterizations by Raman spectroscopy and single-crystal X-ray diffraction of $[\text{XeF}_5][\mu\text{-F}(\text{OsO}_3\text{F}_2)_2]$, $[\text{XeF}_5][\text{OsO}_3\text{F}_3]$, and $[\text{Xe}_2\text{F}_{11}][\text{OsO}_3\text{F}_3]$ are described and provide the first examples of noble-gas cations stabilized by metal oxide fluoride anions. The X-ray crystal structures of these strongly ion-paired salts and their Raman spectra are compared within the series and with the gas-phase ion-pair geometries and vibrational spectra that have been arrived at by quantum-chemical calculations.

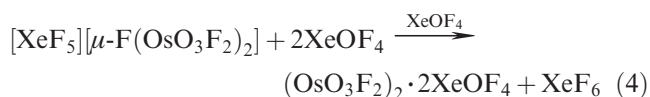
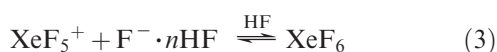
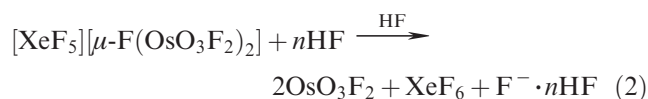
Results and Discussion

Syntheses and Crystal Growth of $[\text{XeF}_5][\mu\text{-F}(\text{OsO}_3\text{F}_2)_2]$, $[\text{XeF}_5][\text{OsO}_3\text{F}_3]$, and $[\text{Xe}_2\text{F}_{11}][\text{OsO}_3\text{F}_3]$. The $[\text{XeF}_5][\mu\text{-F}(\text{OsO}_3\text{F}_2)_2]$, $[\text{XeF}_5][\text{OsO}_3\text{F}_3]$, and $[\text{Xe}_2\text{F}_{11}][\text{OsO}_3\text{F}_3]$ salts were synthesized by direct reaction of XeF_6 and $(\text{OsO}_3\text{F}_2)_\infty$ at temperatures ranging from 25 to 50 °C, and the extent of reaction was monitored by low-temperature (−150 °C) Raman spectroscopy.

A 2:1 molar ratio of OsO_3F_2 and XeF_6 was allowed to react at room temperature (25 °C), initially forming an orange liquid which solidified as the reaction progressed. To ensure complete reaction, the resulting microcrystalline orange solid, $[\text{XeF}_5][\mu\text{-F}(\text{OsO}_3\text{F}_2)_2]$, was heated at 50 °C for 1 h but showed no physical changes or change in the Raman spectrum (eq 1). When dissolved in HF at 25 °C, the fluoride ion affinity of HF was sufficient to abstract a fluoride ion from $\mu\text{-F}(\text{OsO}_3\text{F}_2)_2^-$ to form



$(\text{OsO}_3\text{F}_2)_\infty$, XeF_6 , and $\text{F}^- \cdot n\text{HF}$ (eq 2). In HF solution, XeF_6 ionizes to XeF_5^+ and $\text{F}^- \cdot n\text{HF}$ (eq 3).¹⁴ In XeOF_4 solvent at 25 °C, $[\text{XeF}_5][\mu\text{-F}(\text{OsO}_3\text{F}_2)_2]$ reacted to form $(\text{OsO}_3\text{F}_2)_2 \cdot 2\text{XeOF}_4$ ⁵ and XeF_6 (eq 4) which was verified by Raman spectroscopy after removal of the solvent at −40 °C.



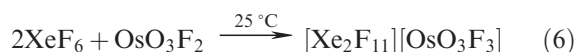
When molten $[\text{XeF}_5][\mu\text{-F}(\text{OsO}_3\text{F}_2)_2]$ was cooled from 50 to 25 °C over a period of 1 h, light orange, block-shaped crystals of $[\text{XeF}_5][\mu\text{-F}(\text{OsO}_3\text{F}_2)_2]$ formed which were suitable for single-crystal X-ray diffraction. The Raman spectrum of the recrystallized compound was identical to that of the bulk microcrystalline compound used for recrystallization.

A 1:1 molar ratio of OsO_3F_2 and XeF_6 was fused at 25 °C, yielding an intense orange liquid that slowly solidified at 0 °C to give an orange crystalline mass that corresponded to $[\text{XeF}_5][\text{OsO}_3\text{F}_3]$ (eq 5). The sample was remelted and slowly cooled over a period of 1 h from 5 to



0 °C, forming light orange block-shaped crystals that were suitable for single-crystal X-ray diffraction. The Raman spectra of the initial crystalline solid and of the remelted crystalline solid were identical.

The reaction of $(\text{OsO}_3\text{F}_2)_\infty$ with two molar equivalents of XeF_6 yielded an orange, microcrystalline powder corresponding to $[\text{Xe}_2\text{F}_{11}][\text{OsO}_3\text{F}_3]$ (eq 6), which melted at 40–45 °C to give an intense orange liquid.



Cooling of the melt to 25 °C resulted in crystalline $[\text{Xe}_2\text{F}_{11}][\text{OsO}_3\text{F}_3]$. Crystalline $[\text{Xe}_2\text{F}_{11}][\text{OsO}_3\text{F}_3]$, suitable for single-crystal X-ray diffraction, was obtained by heating a mixture of 4.6 equiv of XeF_6 and 1 equiv of OsO_3F_2 at 45 °C, whereupon XeF_6 melted and reacted with OsO_3F_2 to form an intense orange liquid. Cooling of the reaction mixture to 15 °C over a period of 12 h resulted in the growth of light orange needle-shaped crystals of $[\text{Xe}_2\text{F}_{11}][\text{OsO}_3\text{F}_3]$ and colorless block-shaped crystals of XeF_6 . The latter was shown to be a monoclinic phase ($P2_1/c$, $Z = 32$) of XeF_6 ^{15,16} based on its unit cell parameters. Crystals grown from the XeF_6 melt had the same unit cell parameters as crystals grown from a 2:1 stoichiometric mixture of $\text{XeF}_6/\text{OsO}_3\text{F}_2$.

The salts, $[\text{XeF}_5][\mu\text{-F}(\text{OsO}_3\text{F}_2)_2]$, $[\text{XeF}_5][\text{OsO}_3\text{F}_3]$, and $[\text{Xe}_2\text{F}_{11}][\text{OsO}_3\text{F}_3]$, are stable at room temperature for up to 24 h; however, when heated at 50 °C under ca. 1 atm of dry N_2 for periods exceeding 2 h, crystals of XeF_6 sublimed out of the heated zone and condensed on the cooler walls of the reaction vessel. Although XeF_6 is oxophilic toward a number of metal oxides and oxide fluorides,^{17–19} fluoride/oxide metathesis, indicated by XeOF_4 formation and strong $\text{Xe}-\text{O}$ stretching bands at 902 and 908 cm^{-1} in the solid,⁵ was not detected in the course of monitoring the aforementioned syntheses by Raman spectroscopy.

(15) Burbank, R. D.; Jones, G. R. *Science* **1971**, *171*, 485–487.

(16) Hoyer, S.; Emmeler, T.; Seppelt, K. *J. Fluorine Chem.* **2006**, *127*, 1415–1422.

(17) Mercier, H. P. A.; Schrobilgen, G. J. *Inorg. Chem.* **1993**, *32*, 145–151.

(18) Fele Beuermann, M.; Miličević, S.; Lutar, K.; Žemva, B. *Eur. J. Solid State Inorg. Chem.* **1994**, *31*, 545–556.

(19) Casteel, W. J.; Dixon, D. A.; LeBlond, N.; Lock, P. E.; Mercier, H. P. A.; Schrobilgen, G. J. *Inorg. Chem.* **1999**, *38*, 2340–2358.

(12) Bougon, R.; Buu, B.; Seppelt, K. *Chem. Ber.* **1993**, *126*, 1331–1336.

(13) Bartlett, N.; Sladky, F. O. *J. Am. Chem. Soc.* **1968**, *90*, 5316–5317.

(14) Hyman, H. H.; Quarterman, L. A. In *Noble-Gas Compounds*; Hyman, H. H., Ed.; University of Chicago Press: Chicago, 1963; pp 275–278.

Table 1. Summary of Crystal Data and Refinement Results for [XeF₅][μ-F(OsO₃F₂)₂], [XeF₅][OsO₃F₃], and [Xe₂F₁₁][OsO₃F₃]

	[XeF ₅][μ-F(OsO ₃ F ₂) ₂]	[XeF ₅][OsO ₃ F ₃]	[Xe ₂ F ₁₁][OsO ₃ F ₃]
chem formula	Os ₈ O ₂₄ F ₄₀ Xe ₄	Os ₈ O ₂₄ F ₆₄ Xe ₈	Os ₄ O ₁₂ F ₅₆ Xe ₈
space group	<i>Pnma</i> (62)	<i>P4₂/n</i> (86)	<i>Pnma</i> (62)
<i>a</i> (Å)	12.672(1)	16.8876(3)	9.2479(3)
<i>b</i> (Å)	11.444(1)	16.8876(3)	15.1769(5)
<i>c</i> (Å)	7.5818(7)	5.3414(2)	8.1192(2)
<i>V</i> (Å ³)	1099.6(2)	1523.3(1)	1139.46(6)
molecules/unit cell	4	8	4
mol wt (g mol ⁻¹)	1633.40	4172.00	3067.20
calcd density (g cm ⁻³)	4.819	4.548	4.470
<i>T</i> (°C)	−173	−173	−173
<i>μ</i> (mm ⁻¹)	26.28	21.24	17.24
<i>R</i> ₁ ^a	0.0273	0.0356	0.0249
<i>wR</i> ₂ ^b	0.0486	0.0729	0.0603

^a *R*₁ is defined as $\sum||F_o| - |F_c|| / \sum|F_o|$ for $I > 2\sigma(I)$. ^b *wR*₂ is defined as $\{\sum w(F_o^2 - F_c^2)^2 / \sum w(F_o^2)\}^{1/2}$ for $I > 2\sigma(I)$.

X-ray Crystal Structures of [XeF₅][μ-F(OsO₃F₂)₂], [XeF₅][OsO₃F₃], and [Xe₂F₁₁][OsO₃F₃]. Details of data collection parameters and other crystallographic information are provided in Table 1. The bond lengths and bond angles of [XeF₅][μ-F(OsO₃F₂)₂] are listed in Table 2 and those of [XeF₅][OsO₃F₃] and [Xe₂F₁₁][OsO₃F₃] are listed in Table 3. Crystal packing diagrams (Figures S1–S3, Supporting Information) along with a brief discussion of the packing arrangements are given in the Supporting Information. The ion pairs of all three structures are well isolated from one another (Figures 1a–3a), although an inter-ion pair contact (O(1B)⋯Xe(1)) occurs in the [Xe₂F₁₁][OsO₃F₃] structure, with long intermolecular contacts between adjacent ion pairs in [XeF₅][μ-F(OsO₃F₂)₂], [XeF₅][OsO₃F₃], and [Xe₂F₁₁][OsO₃F₃] near the sums of the van der Waals radii²⁰ of the contacting atoms.

(a) OsO₃F₃[−] and μ-F(OsO₃F₂)₂[−]. The primary coordination spheres of the osmium atoms in [XeF₅][μ-F(OsO₃F₂)₂], [XeF₅][OsO₃F₃], and [Xe₂F₁₁][OsO₃F₃] consist of three oxygen and three fluorine atoms in facial arrangements, providing distorted octahedral environments around the osmium atoms (Figures 1–3). The preference for the *fac*-trioxo arrangement has been previously discussed for other d⁰ osmium trioxo-species such as (OsO₃F₂)_∞,¹² OsO₃F₃[−],⁴ (OsO₃F₂)₂·2XeOF₄,⁵ and [OsO₃F][HF][SbF₆].²¹ The OsO₃F₂-groups of μ-F(OsO₃F₂)₂[−] are symmetry related, and therefore only one OsO₃F₂-group is discussed.

The [XeF₅][μ-F(OsO₃F₂)₂] salt is the first example of the fluorine-bridged μ-F(OsO₃F₂)₂[−] anion (Figure 1a). The Os–O bond lengths are equal to within ±3σ (1.698(2), 1.701(2), 1.692(2) Å) and are similar to those of the OsO₃F₃[−] anion (vide infra). The F(3) atom bridges the OsO₃F₂-groups, resulting in a bridge bond length (Os(1)---F(3), 2.1179(5) Å) that is similar to the Os---F bridge bond lengths in (OsO₃F₂)_∞ (2.126(1), 2.108(1) Å)¹² and (OsO₃F₂)₂·2XeOF₄ (2.117(5), 2.107(4) Å).⁵ The Os–F(1) and Os–F(2) bond lengths (1.978(1) and 1.962(1) Å, respectively) are significantly shorter than the Os–F bonds of the OsO₃F₃[−] anions in the Xe₂F₁₁⁺ and XeF₅⁺ salts (vide infra). When compared with other terminal Os–F bond lengths of the related fluorine-bridged species (OsO₃F₂)_∞ (1.879(1) Å)¹² and

(OsO₃F₂)₂·2XeOF₄ (1.927(5) Å),⁵ the Os–F bonds of the OsO₃F₃[−] and μ-F(OsO₃F₂)₂[−] anions are elongated as a result of increased negative charge on the oxygen ligands of the anions. The terminal fluorine atoms of μ-F(OsO₃F₂)₂[−], F(1)/F(1A) and F(2)/F(2A), form bridge contacts to xenon of the XeF₅⁺ cation, constraining the symmetry-related OsO₂F₂-equatorial planes of μ-F(OsO₃F₂)₂[−] so that they are eclipsed. Although the Os(1)---F(3)---Os(1A) bridge bond angle (155.5(1)°) is significantly bent, which allows the four fluorine ligands to chelate the XeF₅⁺ cation, it is significantly more open than in the related Os(VIII) compounds, (OsO₃F₂)_∞ (143.9(2)°)¹² and (OsO₃F₂)₂·2XeOF₄ (109(1)°),⁵ owing to the steric requirements of the XeF₅⁺ cation.

The geometrical parameters of the OsO₃F₃[−] anions in the present study (Figures 2 and 3) are in good agreement with those reported for the K⁺³ and N(CH₃)₄⁺⁴ salts. The Os–O bond lengths are equal, within ±3σ, for [Xe₂F₁₁][OsO₃F₃] (1.703(2), 1.697(3) Å) and [XeF₅][OsO₃F₃] (1.701(3), 1.701(3), 1.692(3) Å), and are in good agreement with the values reported for [K][OsO₃F₃] (1.698(2) Å, EXAFS),³ [N(CH₃)₄][OsO₃F₃] (1.70(1)–1.73(1) Å),⁴ (OsO₃F₂)_∞ (1.678(1)–1.727(1) Å),¹² and (OsO₃F₂)₂·2XeOF₄ (1.684(6)–1.703(6) Å).⁵ The Os–F bond lengths of [Xe₂F₁₁][OsO₃F₃] (2.004(2), 2.001(2) Å) and [XeF₅][OsO₃F₃] (2.011(2), 2.006(2), 2.028(2) Å) are also in good agreement with each other, but are somewhat elongated compared to those of [N(CH₃)₄][OsO₃F₃] (1.97(1), 1.91(1), 1.94(1) Å)⁴ and [K][OsO₃F₃] (1.919(15) Å),³ which is attributed to significant Xe⋯F intra-ion pair contacts with the XeF₅⁺ and Xe₂F₁₁⁺ cations (vide infra).

The light atoms of OsO₃F₃[−] and μ-F(OsO₃F₂)₂[−] form relatively undistorted octahedral coordination spheres about the osmium atoms (Figure S4, Supporting Information) as shown by their nearest-neighbor interligand atom contacts (Table S1, Supporting Information). The displacements of the osmium atoms toward the centroid of the three facial oxygen atoms are similar to the metal atom displacements observed for other Os(VIII) compounds, which have been previously discussed in detail for (OsO₃F₂)_∞,¹² (OsO₃F₂)₂·2XeOF₄,⁵ and OsO₃F₃[−].⁴

(b) XeF₅⁺ and Xe₂F₁₁⁺. The XeF₅⁺ cations of [XeF₅][μ-F(OsO₃F₂)₂] (Figure 1) and [XeF₅][OsO₃F₃] (Figure 2) are based on pseudo-octahedral AX₅E VSEPR arrangements of bond pairs (X) and lone pairs (E) which give rise

(20) Bondi, A. J. *Phys. Chem.* **1964**, *68*, 441–451.

(21) Gerken, M.; Dixon, D. A.; Schrobilgen, G. J. *Inorg. Chem.* **2002**, *41*, 259–277.

Table 2. Experimental and Calculated Geometrical Parameters for $[\text{XeF}_5][\mu\text{-F}(\text{OsO}_3\text{F}_2)_2]$

	calcd ^b						
	[XeF ₅][μ-F(OsO ₃ F ₂) ₂]			μ-F(OsO ₃ F ₂) ₂ [−]		XeF ₅ ⁺	
	exptl ^d	C _{2v}		C ₂		C _{4v}	
		SVWN ^c	B3LYP ^d	SVWN ^c	B3LYP ^d	SVWN ^c	B3LYP ^e
Bond Lengths (Å)							
Os(1)–F(1)	1.978(1)	1.975	1.980	1.919	1.927		
Os(1)–F(2)	1.962(1)	1.975	1.980	1.908	1.925		
Os(1)–F(3)	2.1179(5)	2.115	2.147	2.121	2.157		
Os(1)–O(1)	1.698(2)	1.712	1.690	1.729	1.701		
Os(1)–O(2)	1.701(2)	1.712	1.690	1.730	1.702		
Os(1)–O(3)	1.692(2)	1.708	1.690	1.723	1.699		
Xe(1)···F(1)	2.622(1)	2.461	2.643				
Xe(1)···F(2)	2.663(1)	2.461	2.644				
Xe(1)–F(4)	1.822(2)	1.890	1.881			1.844	1.840
Xe(1)–F(5)	1.848(1)	1.922	1.898			1.877	1.871
Xe(1)–F(6)	1.848(2)	1.916	1.902			1.877	1.871
Xe(1)–F(7)	1.852(2)	1.916	1.902			1.877	1.871
Xe(1)–F(5A)	1.848(1)	1.922	1.898			1.877	1.871
Bond Angles (deg)							
F(1)–Os(1)–F(2)	75.71(6)	74.2	74.4	77.6	77.6		
F(1)–Os(1)–F(3)	79.18(7)	77.0	77.4	78.2	78.3		
F(1)–Os(1)–O(1)	160.07(7)	156.6	157.1	158.6	159.1		
F(1)–Os(1)–O(2)	87.72(8)	88.2	88.5	87.6	88.0		
F(1)–Os(1)–O(3)	91.39(8)	93.1	93.2	94.9	94.1		
F(2)–Os(1)–F(3)	77.22(7)	77.0	77.4	79.4	77.8		
F(2)–Os(1)–O(1)	88.99(7)	88.2	88.5	88.4	88.0		
F(2)–Os(1)–O(2)	156.62(7)	156.6	157.1	158.3	158.7		
F(2)–Os(1)–O(3)	94.56(8)	93.1	93.2	95.0	94.4		
F(3)–Os(1)–O(1)	85.10(8)	84.2	84.2	83.5	83.9		
F(3)–Os(1)–O(2)	83.62(8)	84.2	84.2	82.0	84.0		
F(3)–Os(1)–O(3)	168.71(9)	167.5	168.1	171.9	170.0		
O(1)–Os(1)–O(2)	102.72(9)	103.7	103.2	100.8	101.1		
O(1)–Os(1)–O(3)	102.67(9)	103.3	103.0	102.3	102.2		
O(2)–Os(1)–O(3)	102.34(9)	103.3	103.0	102.1	102.2		
F(1)···Xe(1)···F(2)	54.44(4)	57.9	53.8				
F(1)···Xe(1)–F(4)	136.53(6)	135.7	136.9				
F(1)···Xe(1)–F(5)	70.03(5)	70.3	69.8				
F(1)···Xe(1)–F(5A)	130.36(5)	130.2	130.9				
F(1)···Xe(1)–F(6)	126.07(6)	128.1	125.4				
F(1)···Xe(1)–F(7)	71.09(6)	70.6	71.9				
F(2)···Xe(1)–F(4)	135.95(6)	135.7	136.9				
F(2)···Xe(1)–F(5)	68.19(6)	130.2	130.9				
F(2)···Xe(1)–F(5A)	131.94(6)	70.3	69.8				
F(2)···Xe(1)–F(6)	71.81(6)	70.6	71.9				
F(2)···Xe(1)–F(7)	124.98(6)	128.1	125.4				
F(4)–Xe(1)–F(5)	77.96(5)	77.6	77.8			83.1	83.5
F(4)–Xe(1)–F(5A)	77.96(5)	77.6	77.8			83.1	83.5
F(4)–Xe(1)–F(6)	79.7(1)	78.5	79.4			83.1	83.5
F(4)–Xe(1)–F(7)	79.3(1)	78.5	79.4			83.1	83.5
F(5)–Xe(1)–F(5A)	155.91(9)	155.1	155.6			166.2	167.0
F(5)–Xe(1)–F(6)	87.67(5)	87.5	87.8			89.2	89.3
F(5)–Xe(1)–F(7)	87.98(5)	87.5	87.8			89.2	89.3
F(5A)–Xe(1)–F(6)	87.67(5)	87.5	87.8			89.2	89.3
F(5A)–Xe(1)–F(7)	87.98(5)	87.5	87.8			89.2	89.3
F(6)–Xe(1)–F(7)	159.0(1)	157.0	158.9			166.2	167.0
Os(1)–F(3)–Os(1A)	155.5(1)	150.9	155.4	143.0	140.7		
Os(1)–F(1)···Xe(1)	114.94(6)	113.8	115.6				
Os(1)–F(2)···Xe(1)	113.83(6)	113.8	115.6				

^a See Figure 1a for the atom labeling scheme. ^b See Figure 7a for the atom labeling scheme, where F(5A) and Os(1A) correspond to F_{5'} and Os', respectively, for the symmetry-related atoms. ^c The SDDall(-PP) basis set was used augmented for F, O, and Xe with two d-type polarization functions. ^d The Stuttgart basis set was used for Os with the f functional. The aug-cc-pVTZ(-PP) basis sets were used for all other atoms. ^e The aug-cc-pVTZ(-PP) basis sets were used.

to a square-pyramidal geometry. The $\text{Xe}_2\text{F}_{11}^+$ cation of $[\text{Xe}_2\text{F}_{11}][\text{OsO}_3\text{F}_3]$ (Figure 3) is comprised of two XeF_5^+ cations bridged by a common fluoride ion such that the trajectories of the fluorine bridge interactions with the

xenon atoms approach opposite the axial fluorine ligands and from beneath the equatorial planes of the XeF_5 -groups so that the axial lone pairs of the xenon atoms are avoided. The four fluorine atoms that comprise the

Table 3. Experimental and Calculated Geometrical Parameters for [XeF₃][OsO₃F₃] and [Xe₂F₁₁][OsO₃F₃]

	[XeF ₅][OsO ₃ F ₃] ^a			[Xe ₂ F ₁₁][OsO ₃ F ₃] ^b		
		calcd (C _s)			calcd (C _s)	
	exptl	SVWN ^c	B3LYP ^d	exptl	SVWN ^c	B3LYP ^d
Bond Lengths (Å)						
Os—F(1)	2.011(2)	2.032	2.052	2.004(2)	2.018	2.072
Os—F(2)	2.006(2)	2.032	2.052	2.001(2)	2.033	1.949
Os—F(3)	2.028(2)	1.999	1.990			
Os—O(1)	1.701(3)	1.711	1.688	1.703(2)	1.711	1.689
Os—O(2)	1.701(3)	1.711	1.688	1.697(3)	1.710	1.690
Os—O(3)	1.692(3)	1.711	1.689			
Xe(1)⋯F(1)	2.514(2)	2.373	2.460	2.504(2)	2.370	2.404
Xe(1)⋯F(2)	2.521(2)	2.373	2.460	2.800(2)	2.613	3.197
Xe(1)⋯F(3) ^e	2.468(2)	2.420	2.606	2.2953(9)	2.244	2.295
Xe(1)—F(4)	1.819(2)	1.890	1.879	1.830(2)	1.893	1.884
Xe(1)—F(5)	1.866(2)	1.923	1.911	1.859(2)	1.921	1.913
Xe(1)—F(6)	1.862(2)	1.924	1.912	1.873(2)	1.939	1.922
Xe(1)—F(7)	1.866(2)	1.924	1.912	1.873(2)	1.928	1.920
Xe(1)—F(8)	1.864(2)	1.923	1.911	1.862(2)	1.918	1.914
Xe(1)⋯O(1B)				3.353(2)		
Bond Angles (deg)						
F(1)—Os—F(2)	74.4(1)	73.2	73.8	75.77(7)	73.9	76.0
F(1)—Os—F(3/1A)	74.6(1)	72.9	73.8	78.96(9)	76.3	77.8
F(1)—Os—O(1/1A)	159.4(1)	158.7	159.8	162.72(9)	160.2	163.8
F(1)—Os—O(2)	89.8(1)	89.5	89.7	88.5(1)	88.5	84.8
F(1)—Os—O(3/1)	89.3(1)	88.4	87.6	88.31(8)	88.6	88.7
F(2)—Os—F(3/1A)	74.8(1)	72.9	73.8	75.77(7)	73.9	76.0
F(2)—Os—O(1/1A)	88.8(1)	89.5	89.7	89.88(9)	89.7	92.2
F(2)—Os—O(2)	158.6(1)	158.7	159.8	159.5(1)	157.5	155.1
F(2)—Os—O(3/1)	90.8(1)	88.4	87.6	89.88(9)	89.7	92.2
F(3/1A)—Os—O(1/1A)	89.8(1)	90.3	90.8	88.31(8)	88.6	88.7
F(3/1A)—Os—O(2)	87.3(1)	90.3	90.8	88.5(1)	88.5	84.8
F(3/1A)—Os—O(3/1)	160.7(1)	156.5	156.7	162.72(9)	160.2	163.8
O(1/1A)—Os—O(2)	103.0(2)	104.0	103.7	102.9(1)	104.1	103.1
O(1/1A)—Os—O(3/1)	102.9(2)	103.9	103.4	101.4(1)	102.8	103.0
O(2)—Os—O(3/1)	103.6(2)	103.9	103.4	102.9(1)	104.1	103.1
F(1)⋯Xe(1)⋯F(2)	57.69(8)	61.4	60.0	54.90(6)	58.3	50.1
F(1)⋯Xe(1)⋯F(3) ^e	58.87(8)	60.0	57.2	75.37(7)	72.4	71.6
F(1)⋯Xe(1)—F(4)	140.0(1)	147.4	148.3	139.68(7)	140.3	142.6
F(1)⋯Xe(1)—F(5)	71.6(1)	111.7	112.0	127.31(7)	128.5	124.3
F(1)⋯Xe(1)—F(6)	124.4(1)	130.1	128.3	74.43(7)	75.6	75.3
F(1)⋯Xe(1)—F(7)	128.3(1)	84.6	84.5	72.47(6)	70.7	73.4
F(1)⋯Xe(1)—F(8)	74.5(1)	71.5	72.4	125.60(7)	123.1	123.5
F(2)⋯Xe(1)⋯F(3) ^e	58.84(8)	60.0	57.2	61.55(7)	62.4	59.1
F(2)⋯Xe(1)—F(4)	145.5(1)	147.4	148.3	135.39(8)	135.1	138.0
F(2)⋯Xe(1)—F(5)	129.0(1)	71.5	72.4	72.43(8)	70.3	74.3
F(2)⋯Xe(1)—F(6)	116.6(1)	84.6	84.5	67.94(6)	69.1	66.8
F(2)⋯Xe(1)—F(7)	71.8(1)	130.1	128.3	126.22(7)	128.1	122.3
F(2)⋯Xe(1)—F(8)	81.1(1)	111.7	112.0	132.84(7)	131.1	132.5
F(3)⋯Xe(1)—F(4) ^e	150.6(1)	137.2	139.3	144.56(9)	145.9	145.6
F(3)⋯Xe(1)—F(5) ^e	91.6(1)	128.2	126.8	79.08(9)	82.2	78.3
F(3)⋯Xe(1)—F(6) ^e	71.95(9)	71.8	72.4	129.45(8)	130.8	125.9
F(3)⋯Xe(1)—F(7) ^e	104.9(1)	71.8	72.4	118.10(9)	112.2	117.8
F(3)⋯Xe(1)—F(8) ^e	129.5(1)	128.2	126.8	72.96(8)	71.8	74.1
F(4)—Xe(1)—F(5)	79.5(1)	79.7	79.9	79.43(9)	80.1	80.3
F(4)—Xe(1)—F(6)	79.5(1)	79.1	79.5	77.45(8)	78.0	79.0
F(4)—Xe(1)—F(7)	79.8(1)	79.1	79.5	79.10(9)	80.4	80.4
F(4)—Xe(1)—F(8)	79.2(1)	79.7	79.9	78.48(9)	78.6	79.2
F(5)—Xe(1)—F(6)	86.3(1)	87.5	88.1	88.24(9)	89.9	86.8
F(5)—Xe(1)—F(7)	158.9(1)	158.3	159.1	158.37(8)	160.0	160.6
F(5)—Xe(1)—F(8)	91.3(1)	84.5	85.1	88.1(1)	87.9	89.8
F(6)—Xe(1)—F(7)	86.3(1)	92.7	91.4	88.65(8)	90.6	91.0
F(6)—Xe(1)—F(8)	158.6(1)	158.3	159.1	155.91(8)	156.6	158.2
F(7)—Xe(1)—F(8)	88.3(1)	87.5	88.1	85.12(8)	83.8	85.1
Os—F(1)⋯Xe(1)				119.39(7)	117.2	131.2
Os—F(2)⋯Xe(1)				107.48(6)	107.0	102.1
Xe(1)⋯F(3)⋯Xe(2)				135.9(1)	129.3	152.2

^a See Figure 2a for the atom labeling scheme. ^b See Figure 3a for the atom labeling scheme. ^c The SDDall(-PP) basis set, augmented for F, O, and Xe with two d-type polarization functions, was used. ^d The Stuttgart basis set was used for Os with the f functional. The aug-cc-pVTZ(-PP) basis sets were used for all other atoms. ^e The atom labeling scheme refers to the structure of [XeF₃][OsO₃F₃]. In the case of [Xe₂F₁₁][OsO₃F₃], the Xe(1)⋯F(3) notation should read as Xe(1)---F(3).

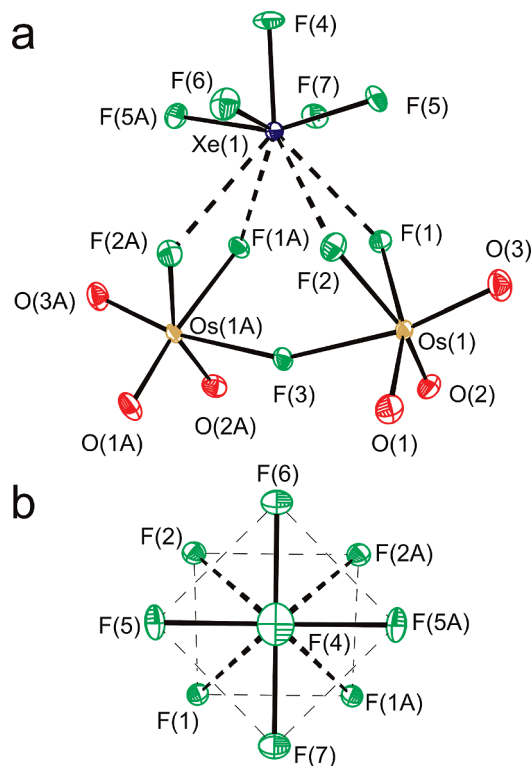


Figure 1. Depictions of (a) the structural unit in the X-ray crystal structure of $[\text{XeF}_5][\mu\text{-F}(\text{OsO}_3\text{F}_2)_2]$ with thermal ellipsoids drawn at the 70% probability level, and (b) the primary and secondary coordination spheres of xenon in XeF_5^+ showing the four secondary bonding interactions between xenon and the terminal fluorine atoms of $\mu\text{-F}(\text{OsO}_3\text{F}_2)_2^-$.

base of the square pyramid are coplanar within ± 0.245 , ± 0.004 , and ± 0.021 Å in $[\text{XeF}_5][\mu\text{-F}(\text{OsO}_3\text{F}_2)_2]$, $[\text{XeF}_5][\text{OsO}_3\text{F}_3]$, and $[\text{Xe}_2\text{F}_{11}][\text{OsO}_3\text{F}_3]$, respectively, and the respective apical fluorine atoms are located 1.460, 1.478, and 1.461 Å above the equatorial plane and the xenon atoms lie 0.362, 0.341, and 0.369 Å below that plane.

The secondary bonding interactions that occur between the cations and anions in all three structures have contact distances that are significantly less than the sum of the xenon and fluorine van der Waals radii,²⁰ resulting in xenon atoms that are eight-coordinate in $[\text{XeF}_5][\text{OsO}_3\text{F}_3]$ (Figure 2b) and nine-coordinate in $[\text{XeF}_5][\mu\text{-F}(\text{OsO}_3\text{F}_2)_2]$ (Figure 1b) and $[\text{Xe}_2\text{F}_{11}][\text{OsO}_3\text{F}_3]$ (Figure 3b). The light atom interatomic distances associated with the xenon coordination spheres are similar, with the distances between the apical fluorine and four equatorial fluorine atoms of the XeF_5 -groups being slightly shorter than the average $\text{F}\cdots\text{F}/\text{O}$ contact distances (Table S1, Supporting Information). All secondary cation–anion contacts are between the fluorine atoms of the anion and the xenon atoms, except in the case of $[\text{Xe}_2\text{F}_{11}][\text{OsO}_3\text{F}_3]$ where an oxygen atom of a neighboring OsO_3F_3^- anion in the unit cell provides an additional short contact to a xenon atom. The anion contacts in all three salts occur from beneath the equatorial planes of the XeF_5 -units so as to avoid the valence electron lone pair position in the manner described for $[\text{XeF}_5][\text{RuF}_6]$.²²

The three long contacts to the XeF_5^+ cation in $[\text{XeF}_5][\text{OsO}_3\text{F}_3]$ occur through the facial fluorine atoms,

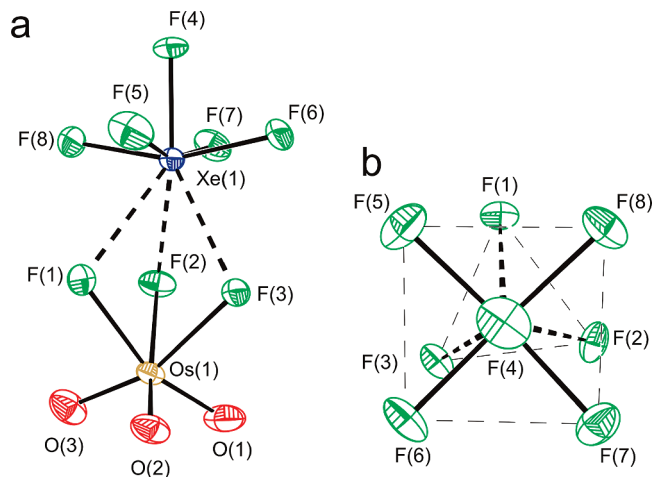


Figure 2. Depictions of (a) the structural unit in the X-ray crystal structure of $[\text{XeF}_5][\text{OsO}_3\text{F}_3]$ with thermal ellipsoids drawn at the 70% probability level, and (b) the primary and secondary coordination spheres of xenon in XeF_5^+ showing the three secondary bonding interactions between xenon and the three facial fluorine atoms of OsO_3F_3^- .

$\text{F}(1,2,3)$, of the anion (Figure 2b), forming a tripod beneath the square base of the XeF_5^+ cation, having very similar $\text{Xe}\cdots\text{F}$ contact distances (2.514(2), 2.521(2), and 2.468(2) Å, respectively). The shortest contact, $\text{Xe}(1)\cdots\text{F}(3)$, is likely a consequence of crystal packing and is reflected in the longer $\text{Os}-\text{F}(3)$ bond (2.028(2) Å) and shorter $\text{Os}-\text{O}(3)$ bond (1.692(3) Å) that is trans to $\text{Os}-\text{F}(3)$. The xenon atom is located 2.064 Å above the $\text{F}(1,2,3)$ -plane which is parallel, to within $\pm 5.2^\circ$, to the equatorial $\text{F}(5,6,7,8)$ -plane of the XeF_5^+ cation. Eight-coordinate xenon has also been observed in other XeF_5^+ salts, for example, $[\text{XeF}_5][\text{PdF}_6]$,²³ $[\text{XeF}_5][\text{AsF}_6]$,²⁴ and $[\text{XeF}_5][\text{NiF}_6]$.²⁵ These examples also contain three long $\text{Xe}\cdots\text{F}$ cation–anion contacts that originate from within the ion pair.

Nine coordination of the xenon atom of XeF_5^+ in $[\text{XeF}_5][\mu\text{-F}(\text{OsO}_3\text{F}_2)_2]$ (Figure 1b) results from four short contacts with the terminal fluorine atoms of the anion (two from each OsO_3F_2 -group) which again contact xenon from beneath the square plane of the cation and avoid the valence electron lone pair. The contact distances are comparable ($\text{Xe}\cdots\text{F}(1,1\text{A})$ (2.622(1) Å) and $\text{Xe}\cdots\text{F}(2,2\text{A})$ (2.663(1) Å)), with the xenon atom located 1.909 Å above the plane defined by the four contacting atoms of the anion, $\text{F}(1,1\text{A},2,2\text{A})$. The four contacting fluorine atoms are coplanar by symmetry and this plane is parallel ($\pm 0.1^\circ$) to the equatorial $\text{F}(5,5\text{A},6,7)$ -plane of XeF_5^+ .

The secondary contacts of the nine-coordinate xenon atoms of $[\text{Xe}_2\text{F}_{11}][\text{OsO}_3\text{F}_3]$ (Figure 3b) do not all originate from within the same ion pair. In the case of $\text{Xe}(1)$, two contacts are with terminal fluorine atoms, $\text{F}(1)$ and $\text{F}(2)$, of the OsO_3F_3^- anion, one is with the bridging $\text{F}(3)$ atom of the $\text{Xe}_2\text{F}_{11}^+$ cation, and the remaining contact is with $\text{O}(1\text{B})$ (3.353(2) Å) of another OsO_3F_3^- anion in the unit cell. The $\text{Xe}(1)\cdots\text{F}(2)$ contact distance (2.800(2) Å)

(23) Leary, K.; Templeton, D. H.; Zalkin, A.; Bartlett, N. *Inorg. Chem.* **1973**, *12*, 1726–1730.

(24) Bartlett, N.; DeBoer, B. G.; Hollander, F. J.; Sladky, F. O.; Templeton, D. H.; Zalkin, A. *Inorg. Chem.* **1974**, *13*, 780–785.

(25) Jesih, A.; Lutar, K.; Leban, I.; Zemva, B. *Eur. J. Solid State Inorg. Chem.* **1991**, *28*, 829–840.

(22) Bartlett, N.; Gennis, M.; Gibling, D. D.; Morrell, B. K.; Zalkin, A. *Inorg. Chem.* **1973**, *12*, 1717–1721.

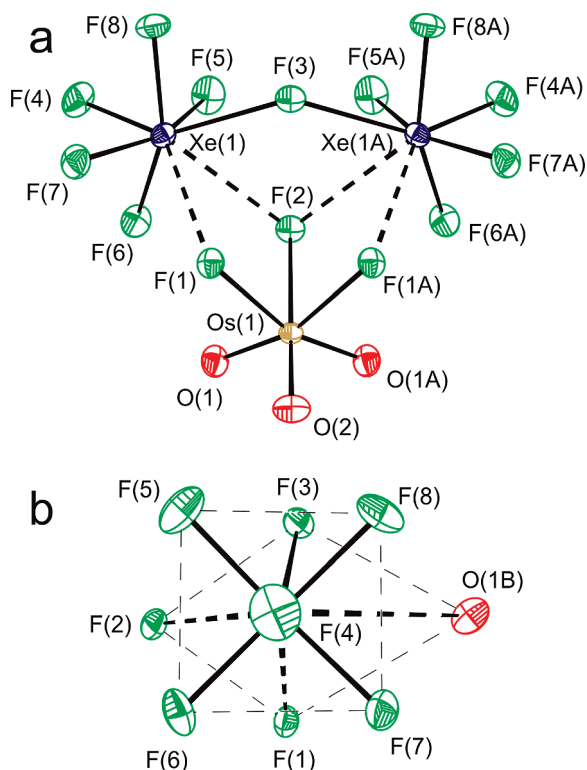


Figure 3. Depictions of (a) the structural unit in the X-ray crystal structure of $[\text{Xe}_2\text{F}_{11}][\text{OsO}_3\text{F}_3]$ with thermal ellipsoids drawn at the 70% probability level, and (b) the primary and secondary coordination spheres of xenon in the XeF_5^+ units of $\text{Xe}_2\text{F}_{11}^+$ showing the secondary bonding interactions between one oxygen atom and three fluorine atoms of OsO_3F_3^- and one xenon atom of $\text{Xe}_2\text{F}_{11}^+$.

is relatively long when compared with $\text{Xe}(1)\cdots\text{F}(1)$ (2.504(2) Å) because F(2) is equivalently coordinated to both Xe(1) and Xe(1A), whereas F(1) forms a single short contact with Xe(1). The Xe(1) atom is located 1.916 Å above the near parallelogram-shaped arrangement of F(1), F(2), F(3), O(1B) atoms, which are coplanar to within ± 0.0260 Å and parallel to the F(5,6,7,8)-plane to within $\pm 2.0^\circ$.

The planes of contacting atoms and the equatorial fluorine atoms of the XeF_5 -groups in $[\text{XeF}_5][\mu\text{-F}(\text{OsO}_3\text{F}_2)_2]$ (Figure 1b) and $[\text{Xe}_2\text{F}_{11}][\text{OsO}_3\text{F}_3]$ (Figure 3b) have near-staggered conformations. The xenon coordination spheres may be described as distorted monocapped square antiprisms having dihedral angles between the basal fluorine atom planes of the XeF_5 -groups and planes of contacting atoms that are close to 45° (49.0° for the F(4,5,7)Xe(1)- and F(1,3,4)Xe(1)-planes and 42.9° for the O(1B)F(2,4)Xe(1)- and F(4,6,8)Xe(1)-planes of $[\text{Xe}_2\text{F}_{11}][\text{OsO}_3\text{F}_3]$; 41.4° for the F(4,5,5A)Xe(1)- and F(1,2A,4)Xe(1)-planes and 48.6° for the F(1A,2,4)Xe(1)- and F(4,6,7)Xe(1)-planes of $[\text{XeF}_5][\mu\text{-F}(\text{OsO}_3\text{F}_2)_2]$). The near-staggered arrangements provide the closest packed arrangements for the fluorine atoms of the equatorial XeF_4 -planes and the light atoms that comprise the secondary coordination sphere. In contrast, the equatorial XeF_4 -planes of $\text{Xe}_2\text{F}_{11}^+$ are eclipsed because they are constrained by symmetry.

Nine-coordinate xenon occurs in other XeF_5^+ and $\text{Xe}_2\text{F}_{11}^+$ salts, for example, $[\text{XeF}_5][\text{SbF}_6]\cdot\text{XeOF}_4$,²⁶

$[\text{XeF}_5][\text{AsF}_6]$,²⁴ $[\text{XeF}_5][\text{PtF}_6]$,²⁷ $[\text{XeF}_5][\text{RuF}_6]$,²² $[\text{XeF}_5][\text{AgF}_4]$,²⁸ $[\text{Xe}_2\text{F}_{11}][\text{AuF}_6]$,²⁹ and $[\text{Xe}_2\text{F}_{11}][\text{NiF}_6]$.³⁰ The xenon coordination in $[\text{Xe}_2\text{F}_{11}][\text{OsO}_3\text{F}_3]$ is similar to that of the AuF_6^- salt where the secondary coordination sphere of xenon also arises from one inter- and two intra-ion pair contacts within the unit cell. The nine-coordination to xenon in $[\text{XeF}_5][\mu\text{-F}(\text{OsO}_3\text{F}_2)_2]$ is, however, unique because it is the only XeF_5^+ salt known to have four secondary fluorine contacts to a XeF_5^+ cation that originate solely from the anion of its ion pair.

With the exception of $\text{Xe}(1)\cdots\text{F}(2)$ in $[\text{Xe}_2\text{F}_{11}][\text{OsO}_3\text{F}_3]$ (2.800(2) Å), the $\text{Xe}\cdots\text{F}$ contact distances in all three salts are shorter than those in $(\text{OsO}_3\text{F}_2)_2\cdot 2\text{XeOF}_4$ (2.757(5) Å),⁵ which is accompanied by significant charge transfer from the anion to the cation (see Computational Results).

Raman Spectroscopy. The low-temperature Raman spectra of $[\text{XeF}_5][\mu\text{-F}(\text{OsO}_3\text{F}_2)_2]$, $[\text{XeF}_5][\text{OsO}_3\text{F}_3]$, and $[\text{Xe}_2\text{F}_{11}][\text{OsO}_3\text{F}_3]$ are shown in Figures 4–6, respectively. The observed and calculated frequencies and mode descriptions for $[\text{XeF}_5][\mu\text{-F}(\text{OsO}_3\text{F}_2)_2]$, $[\text{XeF}_5][\text{OsO}_3\text{F}_3]$, and $[\text{Xe}_2\text{F}_{11}][\text{OsO}_3\text{F}_3]$ are provided in Tables 4–6, respectively, where the atom numbering schemes are given in Figure 7. Spectral assignments for $[\text{XeF}_5][\mu\text{-F}(\text{OsO}_3\text{F}_2)_2]$, $[\text{XeF}_5][\text{OsO}_3\text{F}_3]$, and $[\text{Xe}_2\text{F}_{11}][\text{OsO}_3\text{F}_3]$ were made by comparison with the calculated frequencies and Raman intensities for the energy-minimized gas-phase geometries of their ion pairs, which are in good agreement with experiment at the SVWN and B3LYP levels of theory.

Examination of Tables 4–6 reveals that several bands in the Raman spectra of $[\text{XeF}_5][\mu\text{-F}(\text{OsO}_3\text{F}_2)_2]$, $[\text{XeF}_5][\text{OsO}_3\text{F}_3]$, and $[\text{Xe}_2\text{F}_{11}][\text{OsO}_3\text{F}_3]$ are split into two bands. Factor-group analyses (see Tables S2–S4 and discussion in the Supporting Information) were therefore undertaken to account for these splittings, and are based on analyses of the ion pairs in the crystal structures of these salts. The Raman bands of $[\text{XeF}_5][\mu\text{-F}(\text{OsO}_3\text{F}_2)_2]$ and $[\text{Xe}_2\text{F}_{11}][\text{OsO}_3\text{F}_3]$ are predicted to be factor-group split into two bands, but this splitting is only resolved for two Raman bands of $[\text{Xe}_2\text{F}_{11}][\text{OsO}_3\text{F}_3]$, namely, those occurring at 933/936 and 422/426 cm^{-1} . The Raman bands of $[\text{XeF}_5][\text{OsO}_3\text{F}_3]$ are predicted to be factor-group split into three bands, but splittings are only resolved for bands occurring at 951/955, 946/948, 652/654, 615/617, and 386/390 cm^{-1} , with the third component remaining unresolved.

The mode descriptions provided in Tables 4–6 show that the cation and anion modes are, for the most part, weakly coupled within their respective ion pairs, with the low-frequency deformation modes displaying the greatest degree of coupling.

(a) OsO_3F_3^- and $\mu\text{-F}(\text{OsO}_3\text{F}_2)_2^-$. The vibrational modes of OsO_3F_3^- in $[\text{N}(\text{CH}_3)_4][\text{OsO}_3\text{F}_3]$ have been previously assigned under C_{3v} symmetry, consistent with a weakly ion-paired anion.⁴ The present assignments for

(27) Bartlett, N.; Einstein, F.; Stewart, D. F.; Trotter, J. *J. Chem. Soc. A.* **1967**, 1190–1193.

(28) Lutar, K.; Jesih, A.; Leban, I.; Žemva, B.; Bartlett, N. *Inorg. Chem.* **1989**, *28*, 3467–3471.

(29) Leary, K.; Zalkin, A.; Bartlett, N. *Inorg. Chem.* **1974**, *13*, 775–779.

(30) Jesih, A.; Lutar, K.; Leban, I.; Žemva, B. *Inorg. Chem.* **1989**, *28*, 2911–2914.

(26) Pointner, B. E.; Suontamo, R. J.; Schrobilgen, G. J. *Inorg. Chem.* **2006**, *45*, 1517–1534.

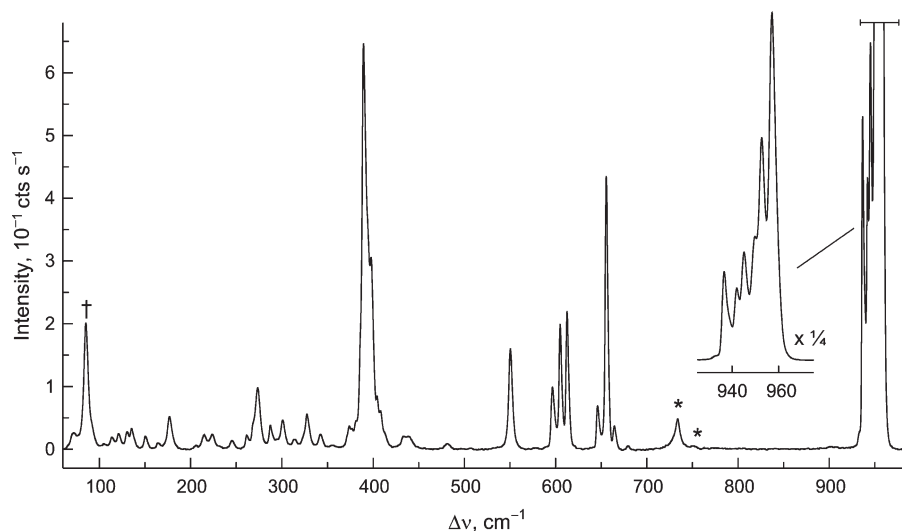


Figure 4. Raman spectrum of $[\text{XeF}_5][\mu\text{-F}(\text{OsO}_3\text{F}_2)_2]$ recorded at -150°C using 1064-nm excitation; the symbols denote FEP sample tube lines (*) and an instrumental artifact (†).

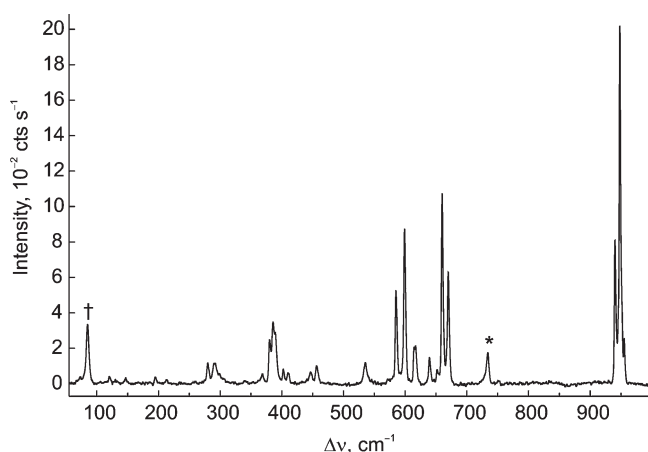


Figure 5. Raman spectrum of $[\text{XeF}_5][\text{OsO}_3\text{F}_3]$ recorded at -150°C using 1064-nm excitation; the symbols denote FEP sample tube lines (*) and an instrumental artifact (†).

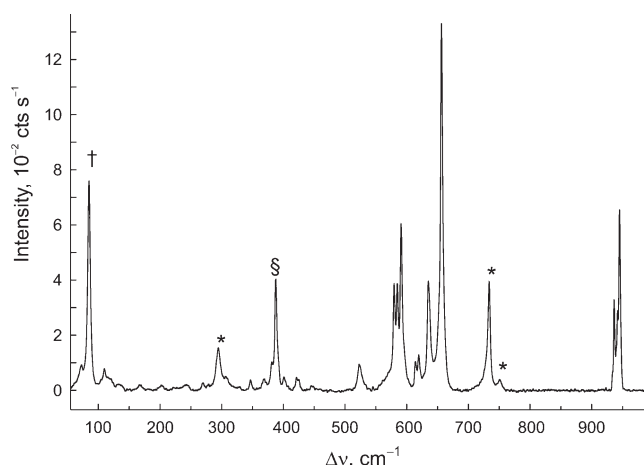


Figure 6. Raman spectrum of $[\text{Xe}_2\text{F}_{11}][\text{OsO}_3\text{F}_3]$ recorded at -150°C using 1064-nm excitation; the symbols denote FEP sample tube lines (*), an instrumental artifact (†), and overlap of a $[\text{Xe}_2\text{F}_{11}][\text{OsO}_3\text{F}_3]$ line with a FEP sample tube line (§).

OsO_3F_3^- in the XeF_5^+ and $\text{Xe}_2\text{F}_{11}^+$ salts are in overall good agreement with the previous assignments; however, strong cation-anion fluorine bridge contacts result in significant vibrational coupling between the anion and the cation modes. These differences are the main focus of the ensuing discussion.

The Os–O stretching frequencies of $[\text{XeF}_5][\mu\text{-F}(\text{OsO}_3\text{F}_2)_2]$ ($933\text{--}957\text{ cm}^{-1}$), $[\text{XeF}_5][\text{OsO}_3\text{F}_3]$ ($940\text{--}955\text{ cm}^{-1}$), and $[\text{Xe}_2\text{F}_{11}][\text{OsO}_3\text{F}_3]$ ($933\text{--}945\text{ cm}^{-1}$) are shifted to higher frequencies when compared with those of the OsO_3F_3^- anion in $[\text{M}][\text{OsO}_3\text{F}_3]$ ($\text{M} = \text{N}(\text{CH}_3)_4^+$ [$908\text{--}920\text{ cm}^{-1}$];⁴ NO^+ [$920\text{--}934\text{ cm}^{-1}$];⁴ Cs^+ [$915\text{--}932\text{ cm}^{-1}$];² Rb^+ [$918\text{--}928\text{ cm}^{-1}$];² K^+ [$916\text{--}932\text{ cm}^{-1}$];² and Na^+ [$920\text{--}935\text{ cm}^{-1}$];²). The high-frequency shifts are in accordance with the presence of several short cation-anion contacts that withdraw negative charge from the anion, leading to more covalent Os–O bonds than in the $\text{N}(\text{CH}_3)_4^+$, NO^+ , and the alkali metal salts. The Os–O stretching modes of $[\text{XeF}_5][\text{OsO}_3\text{F}_3]$ are shifted to somewhat higher frequencies than those of $[\text{Xe}_2\text{F}_{11}][\text{OsO}_3\text{F}_3]$ because secondary bonding interactions with the smaller XeF_5^+ cation are stronger than with the more weakly Lewis acidic $\text{Xe}_2\text{F}_{11}^+$ cation (see

X-ray Crystallography). As expected, the Os–O stretching region of $\mu\text{-F}(\text{OsO}_3\text{F}_2)_2^-$ is more complex than that of OsO_3F_3^- because of vibrational coupling between the two OsO_3F_3^- units. The frequencies of $\mu\text{-F}(\text{OsO}_3\text{F}_2)_2^-$ are in better agreement with those of their counterparts in the neutral species $(\text{OsO}_3\text{F}_2)_\infty$ ($934\text{--}957\text{ cm}^{-1}$),^{5,31,32} $(\text{OsO}_3\text{F}_2)_2$ ($937\text{--}955\text{ cm}^{-1}$),⁵ and $(\text{OsO}_3\text{F}_2)_2 \cdot 2\text{XeOF}_4$ ($940\text{--}962\text{ cm}^{-1}$),⁵ than with those of OsO_3F_3^- (Tables 5 and 6) owing to greater dispersion of negative charge in $\mu\text{-F}(\text{OsO}_3\text{F}_2)_2^-$.

The frequency ranges associated with the terminal Os–F stretching modes of $[\text{XeF}_5][\mu\text{-F}(\text{OsO}_3\text{F}_2)_2]$ ($480\text{--}646\text{ cm}^{-1}$), $[\text{XeF}_5][\text{OsO}_3\text{F}_3]$ ($447\text{--}585\text{ cm}^{-1}$), and $[\text{Xe}_2\text{F}_{11}][\text{OsO}_3\text{F}_3]$ ($422\text{--}591\text{ cm}^{-1}$) salts are similar to the Os–F stretching frequencies of the OsO_3F_3^- anion in its $[\text{M}][\text{OsO}_3\text{F}_3]$ salts ($\text{M} = \text{N}(\text{CH}_3)_4^+$ [$504, 573\text{ cm}^{-1}$];⁴ NO^+

(31) Falconer, W. E.; Disalvo, F. J.; Griffiths, J. E.; Stevie, F. A.; Sunder, W. A.; Vasile, M. J. *J. Fluorine Chem.* **1975**, *6*, 499–520.

(32) Beattie, I. R.; Blayden, H. E.; Crocombe, R. A.; Jones, P. J.; Ogden, J. S. *J. Raman Spectrosc.* **1976**, *4*, 313–322.

Table 4. Experimental Raman and Calculated Frequencies, Intensities, and Assignments for $[\text{XeF}_5][\mu\text{-F}(\text{OsO}_3\text{F}_2)_2]$

exptl ^a	calcd ^b		assgnts (C_{2v}) ^c
	SVWN ^c	B3LYP ^d	
957(100)	991(85)[21]	1027(124)[10]	A_1 , $\nu(\text{OsO}_3) + \nu(\text{Os}'\text{O}_3')$
953(64)	986(2)[141]	1024(<0.1)[93]	B_2 , $\nu(\text{OsO}_3) - \nu(\text{Os}'\text{O}_3')$
950(35)	981(82)[111]	1008(34)[165]	A_1 , $\nu(\text{OsO}_1) + \nu(\text{OsO}_2) + \nu(\text{Os}'\text{O}_1') + \nu(\text{Os}'\text{O}_2')$
945(31)	983(33)[152]	1006(34)[216]	B_1 , $[\nu(\text{OsO}_1) + \nu(\text{Os}'\text{O}_1')] - [\nu(\text{OsO}_2) + \nu(\text{Os}'\text{O}_2')]$
942(20)	978(11)[0]	1003(8)[82]	B_2 , $[\nu(\text{OsO}_1) + \nu(\text{OsO}_2)] - [\nu(\text{Os}'\text{O}_1') + \nu(\text{Os}'\text{O}_2')]$
936(25) 933(sh)	979(5)[0]	1001(3)[0]	A_2 , $[\nu(\text{OsO}_1) + \nu(\text{Os}'\text{O}_2')] - [\nu(\text{OsO}_2) + \nu(\text{Os}'\text{O}_1')]$
680(2)	630(10)[172]	637(7)[174]	B_1 , $\nu(\text{XeF}_6) - \nu(\text{XeF}_7)$
664(2)	619(5)[204]	627(6)[186]	B_2 , $\nu(\text{XeF}_5) - \nu(\text{XeF}_5')$
656(21)	622(58)[54]	621(87)[52]	A_1 , $\nu(\text{XeF}_4)$
646(3)	589(10)[209]	574(7)[80]	A_1 , $\nu(\text{XeF}_4) + \nu(\text{OsF}_1) + \nu(\text{OsF}_2) + \nu(\text{Os}'\text{F}_1') + \nu(\text{Os}'\text{F}_2')$
612(10)	561(20)[34]	563(13)[44]	A_1 , $\nu(\text{XeF}_6) + \nu(\text{XeF}_7)$
605(9)	573(2)[251]	551(3)[273]	B_2 , $[\nu(\text{OsF}_1) + \nu(\text{OsF}_2) + \nu(\text{OsF}_3)] - [\nu(\text{Os}'\text{F}_1') + \nu(\text{Os}'\text{F}_2') + \nu(\text{Os}'\text{F}_3)]$
596(5)	552(41)[68]	550(42)[168]	A_1 , $\nu(\text{XeF}_5) + \nu(\text{XeF}_5')$
550(8)	497(1)[7]	470(1)[15]	B_1 , $[\nu(\text{OsF}_1) + \nu(\text{Os}'\text{F}_1')] - [\nu(\text{OsF}_2) + \nu(\text{Os}'\text{F}_2')]$
480(<1)	477(1)[0]	454(1)[0]	A_2 , $[\nu(\text{OsF}_1) + \nu(\text{Os}'\text{F}_2')] - [\nu(\text{OsF}_2) + \nu(\text{Os}'\text{F}_1')]$
441(1)	473(<1)[21]	452(<1)[25]	B_2 , $\nu(\text{OsF}_3) - \nu(\text{Os}'\text{F}_3)$
433(1)	398(5)[47]	406(6)[1]	A_1 , $\delta(\text{F}_1\text{OsF}_2) + \delta(\text{F}_1'\text{Os}'\text{F}_2') + [\delta(\text{O}_1\text{OsO}_2) + \delta(\text{O}_1'\text{Os}'\text{O}_2')]_{\text{small}}$
409(2)	387(1)[25]	404(2)[7]	B_2 , $[\delta(\text{O}_1\text{OsO}_2) + \delta(\text{F}_1\text{OsF}_2)] - [\delta(\text{O}_1'\text{Os}'\text{O}_2') + \delta(\text{F}_1'\text{Os}'\text{F}_2')]$
405(4)	375(<1)[5]	399(<1)[6]	B_1 , $\rho_t(\text{O}_1\text{OsO}_2) + \delta(\text{O}_1\text{OsO}_3) + \rho_t(\text{O}_1'\text{Os}'\text{O}_2') + \delta(\text{O}_1'\text{Os}'\text{O}_3')$
398(14)	371(2)[1]	398(1)[2]	A_1 , $\delta_{\text{umb}}(\text{OsO}_1\text{O}_2\text{O}_3) + \delta_{\text{umb}}(\text{Os}'\text{O}_1'\text{O}_2'\text{O}_3')$
390(31)	371(9)[0]	395(8)[0]	A_2 , $[\rho_t(\text{O}_1\text{OsO}_2) + \delta(\text{O}_1\text{OsO}_3)] - [\rho_t(\text{O}_1'\text{Os}'\text{O}_2') + \delta(\text{O}_1'\text{Os}'\text{O}_3')]$
	367(3)[19]	394(<1)[29]	B_2 , $\delta_{\text{umb}}(\text{OsO}_1\text{O}_2\text{O}_3) - \delta_{\text{umb}}(\text{Os}'\text{O}_1'\text{O}_2'\text{O}_3')$
382(2)	361(2)[1]	387(3)[23]	B_2 , $\delta(\text{F}_4\text{XeF}_5) - \delta(\text{F}_4\text{XeF}_5')$
374(1)	350(1)[6]	371(1)[8]	B_1 , $\delta(\text{F}_4\text{XeF}_6) - \delta(\text{F}_4\text{XeF}_7)$
342(1)	362(3)[41]	368(1)[32]	A_1 , $\delta(\text{O}_1\text{OsO}_2) + \delta(\text{O}_1'\text{Os}'\text{O}_2') + \nu(\text{OsF}_3) + \nu(\text{Os}'\text{F}_3)$
	337(<1)[<1]	337(1)[72]	A_1 , $\delta_{\text{umb}}(\text{XeF}_1\text{F}_2\text{F}_1'\text{F}_2') + \delta(\text{F}_3\text{XeF}_5') - [\nu(\text{OsF}_3) + \nu(\text{Os}'\text{F}_3)]$
327(2)	331(1)[9]	328(4)[13]	B_2 , $[\delta(\text{O}_1\text{OsO}_2) + \delta(\text{F}_1'\text{Os}'\text{F}_2')] - [\delta(\text{O}_1'\text{Os}'\text{O}_2') + \delta(\text{F}_1\text{OsF}_2)]$
315(1)	313(1)[78]	320(<1)[92]	A_1 , $\rho_w(\text{F}_3'\text{XeF}_5) + \rho_w(\text{F}_6\text{XeF}_7) + \nu(\text{OsF}_3) + \nu(\text{Os}'\text{F}_3)$
	314(<1)[16]	319(<1)[20]	B_1 , $\rho_t(\text{O}_1\text{OsO}_2) + \rho_t(\text{O}_1'\text{Os}'\text{O}_2') + \rho_t(\text{F}_1\text{OsF}_2) + \rho_t(\text{F}_1'\text{Os}'\text{F}_2') + \delta(\text{OsF}_3\text{Os})$
301(2)	290(1)[0]	281(1)[<0.1]	A_2 , $\rho_t(\text{O}_1\text{OsO}_2) + \rho_t(\text{F}_1\text{OsF}_2) - [\rho_t(\text{O}_1'\text{Os}'\text{O}_2') + \rho_t(\text{F}_1'\text{Os}'\text{F}_2')]$
288(2)	266(2)[18]	267(1)[4]	A_1 , $\delta(\text{O}_3\text{OsF}_3) + \delta(\text{O}_3'\text{Os}'\text{F}_3)$
274(4)	247(1)[0]	267(1)[0]	A_2 , $\delta(\text{F}_5\text{XeF}_7) + \delta(\text{F}_6\text{XeF}_5')$
268(sh)	287(<1)[1]	259(<1)[8]	B_1 , $\delta(\text{F}_1\text{XeF}_1') - \delta(\text{F}_2\text{XeF}_2') + \delta(\text{OsF}_3\text{Os})$
262(1)	262(1)[51]	258(1)[75]	B_2 , $\rho_w(\text{F}_1\text{OsF}_2) + \rho_w(\text{F}_1'\text{Os}'\text{F}_2')$
245(1)	241(<1)[<1]	249(<0.1)[<0.1]	A_1 , $\rho_t(\text{F}_5\text{XeF}_6) + \rho_t(\text{F}_5'\text{XeF}_7)$
224(1)	212(<0.1)[<1]	217(<0.1)[<0.1]	B_1 , $\rho_w(\text{F}_5\text{XeF}_5') + \delta(\text{OsF}_3\text{Os}) + \rho_t(\text{F}_1\text{OsF}_2) - \rho_t(\text{F}_1'\text{Os}'\text{F}_2')$
217(1)	180(<0.1)[<1]	198(<0.1)[1]	B_2 , $\delta(\text{F}_6\text{XeF}_7)$
207(<1)	183(<1)[0]	190(<0.1)[0]	A_2 , $\rho_t(\text{F}_1\text{OsF}_2) + \rho_t(\text{F}_2'\text{Os}'\text{F}_1')$
177(2)	172(<1)[<0.1]	185(<1)[<0.1]	} B_1, B_2 , $[\text{XeF}_3][\mu\text{-F}(\text{OsO}_3\text{F}_2)]$ def.
165(<1)	140(<1)[4]	140(1)[8]	
150(1)	154(8)[2]	132(1)[13]	A_1 , $[\text{XeF}_5][\mu\text{-F}(\text{OsO}_3\text{F}_2)]$ breathing mode
136(1)	130(<1)[0]	129(<0.1)[0]	A_2 , $\mu\text{-F}(\text{OsO}_3\text{F}_2)^-$ def.
130(1)	123(1)[2]	114(<1)[2]	B_2 , $[\text{XeF}_3][\mu\text{-F}(\text{OsO}_3\text{F}_2)]$ def.
121(1)	124(1)[<0.1]	106(1)[<0.1]	B_1 , $\mu\text{-F}(\text{OsO}_3\text{F}_2)^-$ breathing mode
114(1)	127(<1)[<0.1]	110(<1)[<0.1]	A_1 , $\rho_t(\text{F}_4\text{XeF}_6) + \rho_t(\text{F}_4\text{XeF}_7)$
92(sh)	105(<1)[1]	93(<1)[6]	A_1 , $[\text{XeF}_5][\mu\text{-F}(\text{OsO}_3\text{F}_2)]$ breathing mode
	95(<0.1)[0]	81(<0.1)[0]	A_2 , $[\text{XeF}_5][\mu\text{-F}(\text{OsO}_3\text{F}_2)]$ def.
	99(<0.1)[<0.1]	63(<0.1)[<1]	} B_1 , $\mu\text{-F}(\text{OsO}_3\text{F}_2)$ def.
	69(<0.1)[<1]	57(<0.1)[<1]	
	59(<0.1)[<0.1]	47(<0.1)[1]	} A_2, B_2 , $[\text{XeF}_5][\mu\text{-F}(\text{OsO}_3\text{F}_2)]$ def.
	72(<0.1)[0]	33(<0.1)[0]	

^a The Raman spectrum was recorded on a microcrystalline solid sample in a FEP tube at -150°C using 1064-nm excitation. Experimental Raman intensities are given in parentheses and are relative intensities with the most intense band given as 100. The abbreviations denote shoulder (sh). ^b Values in parentheses denote calculated Raman intensities ($\text{\AA}^4 \text{u}^{-1}$) and values in square brackets denote calculated infrared intensities (km mol^{-1}). ^c SVWN/SDDall(-PP). ^d B3LYP/Stuttgart (Os) aug-cc-pVTZ(-PP) (Xe, O, F). ^e Assignments are for the energy-minimized geometry calculated at the SVWN level of theory. See Figure 7a for the atom labeling scheme. The symbols denote stretch (ν), bend (δ), twist (ρ_t), rock (ρ_r), wag (ρ_w), and umbrella (δ_{umb}). The abbreviation, def., denotes a deformation mode.

$[\text{555 cm}^{-1}]$,⁴ Cs^+ $[\text{482, 565 cm}^{-1}]$,² Rb^+ $[\text{490, 568 cm}^{-1}]$,² K^+ $[\text{478, 490, 570 cm}^{-1}]$,² Na^+ $[\text{460, 490, 580 cm}^{-1}]$,² and occur at lower frequencies than those of the neutral species, $(\text{OsO}_3\text{F}_2)_\infty$ $[\text{596, 610 cm}^{-1}]$ and $(\text{OsO}_3\text{F}_2)_2$ $[\text{604 cm}^{-1}]$.⁵ The 646 ($[\text{XeF}_5][\mu\text{-F}(\text{OsO}_3\text{F}_2)_2]$) and 591 ($[\text{Xe}_2\text{F}_{11}][\text{OsO}_3\text{F}_3]$) cm^{-1} bands involve coupled terminal Os–F and Xe–F stretches which result in shifts to higher frequency when compared with the pure terminal Os–F stretching frequencies of $[\text{XeF}_5][\mu\text{-F}(\text{OsO}_3\text{F}_2)_2]$ and $[\text{Xe}_2\text{F}_{11}][\text{OsO}_3\text{F}_3]$.

The symmetric Os–F stretches of the terminal OsF_2 groups of $[\text{XeF}_5][\mu\text{-F}(\text{OsO}_3\text{F}_2)_2]$ (646 cm^{-1}) are in-

phase coupled with the axial Xe–F stretch which is shifted to significantly higher frequency than the symmetric Os–F stretch of $[\text{XeF}_5][\text{OsO}_3\text{F}_3]$ (585 cm^{-1}) and $[\text{Xe}_2\text{F}_{11}][\text{OsO}_3\text{F}_3]$ (591 cm^{-1}). The in-phase terminal Os–F stretch of $[\text{Xe}_2\text{F}_{11}][\text{OsO}_3\text{F}_3]$ is weakly coupled to all of the terminal Xe–F stretches of the $\text{Xe}_2\text{F}_{11}^+$ cation whereas the symmetric Os–F stretch of the OsF_3 moiety of $[\text{XeF}_5][\text{OsO}_3\text{F}_3]$ is not significantly coupled to any other mode, and is in good agreement with the symmetric terminal Os–F stretching modes of $[\text{N}(\text{CH}_3)_4][\text{OsO}_3\text{F}_3]$ (573 cm^{-1}),⁴ $(\text{OsO}_3\text{F}_2)_\infty$ (596 cm^{-1}),⁵ and $(\text{OsO}_3\text{F}_2)_2$ (604 cm^{-1}).⁵

Table 5. Experimental Raman and Calculated Frequencies, Intensities, and Assignments for [XeF₅][OsO₃F₃]

exptl ^a	calcd ^b		assgnts (C _s) ^c
	SVWN ^c	B3LYP ^d	
955(12), 951(sh)	986(22)[84]	1008(23)[120]	A'', ν(OsO ₁) – ν(OsO ₂)
948(100), 946(sh)	983(55)[51]	1025(59)[53]	A', ν(OsO ₁) + ν(OsO ₂) + ν(OsO ₃)
940(39)	985(27)[81]	1006(20)[120]	A', ν(OsO ₁) + ν(OsO ₂) – ν(OsO ₃)
654(sh), 652(4)	625(8)[202]	621(8)[208]	A'', [ν(XeF ₅) + ν(XeF ₆)] – [ν(XeF ₇) + ν(XeF ₈)]
670(32)	624(11)[197]	620(7)[204]	A', [ν(XeF ₅) + ν(XeF ₈)] – [ν(XeF ₆) + ν(XeF ₇)]
660(53)	622(58)[148]	619(86)[120]	A', ν(XeF ₄)
617(11), 615(10)	572(16)[12]	569(22)[6]	A', ν(XeF ₄) – [ν(XeF ₅) + ν(XeF ₆) + ν(XeF ₇) + ν(XeF ₈)]
599(44)	556(13)[<0.1]	551(16)[<0.1]	A'', [ν(XeF ₅) + ν(XeF ₇)] – [ν(XeF ₆) + ν(XeF ₈)]
585(27)	551(20)[149]	537(13)[171]	A', ν(OsF ₁) + ν(OsF ₂) + ν(OsF ₃)
457(5)	458(2)[7]	443(2)[12]	A', [ν(OsF ₁) + ν(OsF ₂)] – ν(OsF ₃)
447(3)	445(2)[7]	419(3)[7]	A'', ν(OsF ₁) – ν(OsF ₂)
411(3)	374(3)[4]	397(3)[3]	A'', ρ _t (O ₁ OsO ₃) – δ(O ₂ OsO ₃)
402(4)	364(2)[25]	396(3)[3]	A', δ _{umb} (OsO ₁ O ₂ O ₃)
390(14), 386(18)	371(3)[4]	393(4)[5]	A', δ(O ₁ OsO ₂)
380(12)	399(1)[195]	370(1)[181]	A', ν(Xe···F ₁) + ν(Xe···F ₂) + ν(Xe···F ₃)
369(3)	336(2)[6]	361(1)[7]	A'', δ(F ₄ XeF ₅ F ₆) – ρ _w (F ₇ XeF ₈)
	333(2)[7]	360(1)[19]	A', δ(F ₄ XeF ₅ F ₈) – ρ _w (F ₆ XeF ₇)
291(6)	289(2)[31]	318(3)[61]	A', δ _{umb} (XeF ₅ F ₆ F ₇ F ₈)
299(3)	314(<1)[5]	305(<1)[19]	A'', ρ _t (O ₂ OsO ₃) + ρ _t (F ₁ XeF ₂) + ρ _t (F ₂ XeF ₃)
	277(<1)[6]	292(<1)[30]	A', ρ _w (F ₁ OsF ₂) – [δ(O ₃ OsF ₃) + ρ _w (O ₁ OsO ₂)]
	284(<1)[6]	282(1)[1]	A'', ρ _t (F ₁ OsF ₂) + ρ _w (F ₁ OsF ₃)
280(6)	309(2)[12]	278(1)[2]	A', δ(F ₁ OsF ₂) + δ(F ₃ OsO ₃) + ν(XeF ₃)
213(1)	234(2)[<1]	257(2)[<1]	A', δ(F ₅ XeF ₈) + δ(F ₆ XeF ₇)
	219(<0.1)[<0.1]	231(<0.1)[<0.1]	A'', ρ _t (F ₅ XeF ₆) + ρ _t (F ₇ XeF ₈)
195(2)	172(<1)[<1]	191(<1)[<1]	A'', δ(F ₅ XeF ₆) – δ(F ₇ XeF ₈)
146(2)	167(1)[1]	183(<1)[<1]	A', δ(F ₅ XeF ₈) – δ(F ₆ XeF ₇)
	147(<0.1)[<0.1]	163(<0.1)[<0.1]	A', ρ _{twist} (OsO ₁ O ₂ O ₃) – ρ _{twist} (OsF ₁ F ₂ F ₃)
130(1)	149(2)[4]	133(1)[13]	A', [XeF ₅][OsO ₃ F ₃] breathing
120(2)	112(<1)[<0.1]	112(<1)[<0.1]	A'', [XeF ₅][OsO ₃ F ₃] def.
	102(<1)[<1]	103(<1)[1]	A', ρ _w (F ₄ XeF ₅ F ₈) + ρ _w (F ₆ XeF ₇)
	88(<0.1)[<0.1]	68(<0.1)[<1]	A', ρ _t (O ₁ OsO ₂) + ρ _t (F ₁ OsF ₂) + ρ _t (O ₃ OsF ₃)
	89(<1)[<0.1]	50(<0.1)[<1]	A', ρ _w (O ₁ OsO ₂) + ρ _t (O ₃ OsF ₃) – ρ _w (F ₁ OsF ₂)
	7(<0.1)[<0.1]	21(<0.1)[<0.1]	A'', [XeF ₅][OsO ₃ F ₃] def.

^a The Raman spectrum was recorded on a microcrystalline solid sample in a FEP tube at –150 °C using 1064-nm excitation. Experimental Raman intensities are given in parentheses and are relative intensities with the most intense band given as 100. The abbreviations denote shoulder (sh). Bands were also observed at 536(6) and 639(7) cm^{–1} but were not assigned. ^b Values in parentheses denote calculated Raman intensities (Å⁴ u^{–1}) and values in square brackets denote calculated infrared intensities (km mol^{–1}). ^c SVWN/SDDall(-PP). ^d B3LYP/ Stuttgart (Os) aug-cc-pVTZ(-PP) (Xe, O, F). ^e Assignments are for the energy-minimized geometry calculated at the B3LYP level of theory. See Figure 7b for the atom labeling scheme. The symbols denote stretch (ν), bend (δ), twist (ρ_t), rock (ρ_r), wag (ρ_w), and umbrella (δ_{umb}). The abbreviation, def., denotes a deformation mode.

The asymmetric fluorine bridge stretching mode, ν(OsF₃) – ν(Os'F₃) (441 cm^{–1}), of the μ-F(OsO₃F₂)₂[–] anion is not significantly coupled to any other mode and is comparable to the two asymmetric fluorine bridge stretching modes of (OsO₃F₂)_∞ (404, 413 cm^{–1}).⁵ Upon anion formation, a shift to lower frequency relative to those of (OsO₃F₂)_∞ would be expected for this mode; however, this is not observed and can be attributed to significant withdrawal of electron density from F₁ and F₂ by the XeF₅⁺ cation which strengthens the Os---F bridge bonds. In contrast, the symmetric ν(OsF₃) + ν(Os'F₃) stretch is in-phase coupled to the ρ_w(F₅'XeF₅) + ρ_w(F₆XeF₇) bending mode (313 [SVWN] and 320 [B3LYP] cm^{–1}) and is out-of-phase coupled to the δ_{umb}(XeF₁F₂F₁'F₂') + δ(F₅XeF₅') (337 [SVWN], 337 [B3LYP] cm^{–1}) bending mode of XeF₅⁺. Only the in-phase coupled mode was observed at 315 cm^{–1}. The ν(OsF₃) + ν(Os'F₃) stretch is also in-phase coupled to the δ(O₁OsO₂) + δ(O₁'Os'O₂') mode of μ-F(OsO₃F₂)₂[–] (342 cm^{–1}). These modes are shifted to lower frequency than the pure ν(OsF₃) – ν(Os'F₃) mode as a consequence of coupling with lower frequency OOsO deformation modes.

The asymmetric ν(OsF₁) + ν(OsF₂) – ν(OsF₃) modes of [XeF₅][OsO₃F₃] (457 cm^{–1}) and [Xe₂F₁₁][OsO₃F₃] (448 cm^{–1}) have similar frequencies and are not significantly

coupled to other vibrational modes. The ν(OsF₁) – ν(OsF₂) stretching mode of [XeF₅][OsO₃F₃] (447 cm^{–1}) also is not coupled to any other mode and occurs at higher frequency than the ν(OsF₁) – ν(OsF₁') + ρ_r(O₁OsO₁') + δ(O₂OsO₁') mode of [Xe₂F₁₁][OsO₃F₃] (426/422 cm^{–1}) as a result of coupling with lower frequency OOsO and FXeF bending modes.

(b) XeF₅⁺. Because vibrational assignments for the XeF₅⁺ cation under C_{4v} symmetry have been previously reported for other salts, e.g., AsF₆[–],^{33–35} AuF₆[–],³⁵ BF₄[–],^{34,35} GaF₄[–],³⁶ NiF₆^{2–},²⁵ PdF₆^{2–},³⁵ PtF₆[–],³⁵ RuF₆[–],³⁵ and are in good agreement with the present values for the μ-F(OsO₃F₂)₂[–] (C_{2v} ion-pair symmetry, Table 4) and OsO₃F₃[–] (C_s ion-pair symmetry, Table 5) salts, no detailed discussion of their vibrational assignments is provided. It is noteworthy that the bands at 280 and 380 cm^{–1} in the Raman spectrum of [XeF₅][OsO₃F₃] are

(33) Landa, B. Raman Spectroscopic Investigations of Some Fluoro-xenon Compounds. Ph.D. Thesis, McMaster University, Hamilton, Ontario, 1974.

(34) Christie, K. O.; Curtis, E. C.; Wilson, R. D. in *J. Inorg. Nucl. Chem. Supplement* **1976**, 12, 159–165.

(35) Adams, C. J.; Bartlett, N. *Isr. J. Chem.* **1978**, 17, 114–125.

(36) Zemva, B.; Miličević, S.; Slivnik, J. *J. Fluorine Chem.* **1978**, 11, 519–526.

Table 6. Experimental Raman and Calculated Frequencies, Intensities, and Assignments for $[\text{Xe}_2\text{F}_{11}][\text{OsO}_3\text{F}_3]$

exptl ^a	calcd ^b		assgnts (C _s) ^c
	SVWN ^c	B3LYP ^d	
945(49)	982(59)[43]	1023(58)[50]	A', $\nu(\text{OsO}_1) + \nu(\text{OsO}_2) + \nu(\text{OsO}_1')$
942(21)	983(13)[81]	1006(19)[132]	A'', $\nu(\text{OsO}_1) - \nu(\text{OsO}_1')$
936(24) 933(sh)	986(33)[76]	1001(21)[111]	A', $\nu(\text{OsO}_1) + \nu(\text{OsO}_1') - \nu(\text{OsO}_2)$
	635(8)[248]	622(28)[251]	A', $[\nu(\text{Xe}_1\text{F}_3) + \nu(\text{Xe}_1\text{F}_3')] - [\nu(\text{Xe}_1\text{F}_7) + \nu(\text{Xe}_1\text{F}_7')]$
656(100)	624(105)[192]	620(131)[134]	A', $\nu(\text{Xe}_1\text{F}_4) + \nu(\text{Xe}_1\text{F}_5) + \nu(\text{Xe}_1\text{F}_6) + \nu(\text{Xe}_1\text{F}_4') + \nu(\text{Xe}_1\text{F}_5') + \nu(\text{Xe}_1\text{F}_6')$
635(28)	626(23)[283]	615(39)[399]	A', $[\nu(\text{Xe}_1\text{F}_4) + \nu(\text{Xe}_1\text{F}_6) + \nu(\text{Xe}_1\text{F}_4') + \nu(\text{Xe}_1\text{F}_6')] - [\nu(\text{Xe}_1\text{F}_8) + \nu(\text{Xe}_1\text{F}_8')]$
620(8)	613(12)[37]	609(25)[14]	A'', $[\nu(\text{Xe}_1\text{F}_4) + \nu(\text{Xe}_1\text{F}_5)] - [\nu(\text{Xe}_1\text{F}_4') + \nu(\text{Xe}_1\text{F}_5')]$
613(6)	612(21)[196]	607(14)[121]	$\left\{ \begin{array}{l} \text{A'', } [\nu(\text{Xe}_1\text{F}_4) + \nu(\text{Xe}_1\text{F}_7) + \nu(\text{Xe}_1\text{F}_8) + \nu(\text{Xe}_1\text{F}_5') + \nu(\text{Xe}_1\text{F}_6')] - \\ \quad [\nu(\text{Xe}_1\text{F}_5) + \nu(\text{Xe}_1\text{F}_6) + \nu(\text{Xe}_1\text{F}_4') + \nu(\text{Xe}_1\text{F}_7') + \nu(\text{Xe}_1\text{F}_8')] \\ \text{A'', } [\nu(\text{Xe}_1\text{F}_4) + \nu(\text{Xe}_1\text{F}_6) + \nu(\text{Xe}_1\text{F}_8)] - [\nu(\text{Xe}_1\text{F}_8) + \nu(\text{Xe}_1\text{F}_4') + \nu(\text{Xe}_1\text{F}_6')] \\ \text{A'', } [\nu(\text{Xe}_1\text{F}_3)] + \nu(\text{Xe}_1\text{F}_5) + \nu(\text{Xe}_1\text{F}_6) + \nu(\text{Xe}_1\text{F}_7)] - [\nu(\text{Xe}_1\text{F}_3) + \nu(\text{Xe}_1\text{F}_5') + \nu(\text{Xe}_1\text{F}_6') + \nu(\text{Xe}_1\text{F}_7')] \end{array} \right.$
	604(6)[147]	599(1)[192]	
	569(3)[<1]	568(7)[11]	
591(44)	573(22)[33]	567(20)[52]	$\left\{ \begin{array}{l} \text{A', } [\nu(\text{OsF}_1) + \nu(\text{OsF}_2) + \nu(\text{OsF}_1') + \nu(\text{Xe}_1\text{F}_4) + \nu(\text{Xe}_1\text{F}_4')] - \\ \quad [\nu(\text{Xe}_1\text{F}_5) + \nu(\text{Xe}_1\text{F}_6) + \nu(\text{Xe}_1\text{F}_7) + \nu(\text{Xe}_1\text{F}_8) + \nu(\text{Xe}_1\text{F}_5') + \nu(\text{Xe}_1\text{F}_6') + \nu(\text{Xe}_1\text{F}_7') + \nu(\text{Xe}_1\text{F}_8')] \\ \text{A', } \nu(\text{OsF}_2) \end{array} \right.$
585(27)	529(33)[109]	551(21)[111]	
580(27)	554(13)[29]	544(23)[3]	
	549(5)[<0.1]	542(8)[<1]	A', $[\nu(\text{Xe}_1\text{F}_5) + \nu(\text{Xe}_1\text{F}_7) + \nu(\text{Xe}_1\text{F}_5') + \nu(\text{Xe}_1\text{F}_7')] - [\nu(\text{Xe}_1\text{F}_6) + \nu(\text{Xe}_1\text{F}_8) + \nu(\text{Xe}_1\text{F}_6') + \nu(\text{Xe}_1\text{F}_8')]$
448(1)	435(2)[3]	434(3)[137]	A', $\nu(\text{OsF}_1) + \nu(\text{OsF}_1') - \nu(\text{OsF}_2)$
426(2) 422(3)	453(<1)[113]	412(2)[95]	A'', $\nu(\text{OsF}_1) - \nu(\text{OsF}_1') + \rho_{\text{t}}(\text{O}_1\text{OsO}_1') + \delta(\text{O}_2\text{OsO}_1')$
401(3)	379(3)[32]	400(2)[4]	A', $\rho_{\text{w}}(\text{O}_1\text{OsO}_1') + \rho_{\text{t}}(\text{O}_2\text{OsF}_2)$
386(30) ^f	381(4)[3]	394(4)[23]	A', $\delta(\text{O}_1\text{OsO}_1')$
381(7)	384(4)[110]	388(1)[80]	A'', $\rho_{\text{t}}(\text{O}_1\text{OsO}_1') + \rho_{\text{t}}(\text{F}_1\text{OsF}_1') - \rho_{\text{t}}(\text{O}_2\text{OsF}_2)$
369(2)	344(1)[3]	366(<1)[13]	A', $[\delta(\text{F}_4\text{Xe}_1\text{F}_6) + \delta(\text{F}_4'\text{Xe}_1'\text{F}_6')] - [\delta(\text{F}_4\text{Xe}_1\text{F}_8) + \delta(\text{F}_4'\text{Xe}_1'\text{F}_8')]$
	342(1)[61]	365(1)[4]	A'', $[\delta(\text{F}_3\text{Xe}_1\text{F}_8) + \delta(\text{F}_4\text{Xe}_1\text{F}_6)] - [\delta(\text{F}_3\text{Xe}_1'\text{F}_8') + \delta(\text{F}_4'\text{Xe}_1'\text{F}_6')]$
	362(1)[37]	349(<1)[39]	A', $\delta(\text{OsF}_1\text{F}_2\text{F}_1')$
	319(<1)[8]	347(<1)[62]	A'', $[\delta(\text{F}_4\text{Xe}_1\text{F}_7) + \delta(\text{F}_3\text{Xe}_1\text{F}_5)] - [\delta(\text{F}_3'\text{Xe}_1'\text{F}_5') + \delta(\text{F}_4'\text{Xe}_1'\text{F}_7')]$
347(2)	322(3)[7]	344(1)[1]	A', $[\delta(\text{F}_4\text{Xe}_1\text{F}_5) + \delta(\text{F}_4'\text{Xe}_1'\text{F}_5')] - [\delta(\text{F}_4\text{Xe}_1\text{F}_7) + \delta(\text{F}_4'\text{Xe}_1'\text{F}_7')]$
	370(2)[132]	329(<0.1)[126]	A'', $\nu(\text{XeF}_3) - \nu(\text{Xe}_1'\text{F}_3) + \rho_{\text{t}}(\text{F}_1\text{OsF}_1') + \rho_{\text{w}}(\text{F}_3\text{OsO}_2)$
	335(2)[9]	322(7)[12]	A', $\delta_{\text{umb}}(\text{Xe}_1\text{F}_{4\text{e}}) + \delta_{\text{umb}}(\text{Xe}_1'\text{F}_{4\text{e}}') + \nu(\text{Xe}_1\text{F}_3) + \nu(\text{Xe}_1'\text{F}_3')$
	308(2)[18]	312(1)[92]	A'', $\delta_{\text{umb}}(\text{Xe}_1\text{F}_{4\text{e}}) - \delta_{\text{umb}}(\text{Xe}_1'\text{F}_{4\text{e}}')$
306(3)	313(4)[11]	299(6)[19]	A', $\delta(\text{F}_1\text{OsF}_1') + \delta(\text{F}_2\text{OsO}_2)$
	300(<1)[26]	276(<1)[118]	A', $\nu(\text{Xe}_1\text{F}_3) - \nu(\text{Xe}_1'\text{F}_3) + \rho_{\text{t}}(\text{O}_1\text{OsO}_1') + \rho_{\text{t}}(\text{F}_1\text{OsF}_1')$
	284(2)[28]	257(1)[7]	A', $\rho_{\text{w}}(\text{F}_3\text{Xe}_1\text{F}_7) + \rho_{\text{w}}(\text{F}_3\text{Xe}_1'\text{F}_7') + \delta_{\text{t}}(\text{F}_1\text{OsF}_1')$
269(2)	254(1)[7]	256(4)[13]	A', $\delta(\text{F}_5\text{Xe}_1\text{F}_8) + \delta(\text{F}_6\text{Xe}_1\text{F}_7) + \delta(\text{F}_5'\text{Xe}_1'\text{F}_8) + \delta(\text{F}_6'\text{Xe}_1'\text{F}_7') + \delta(\text{Xe}_1\text{F}_3\text{Xe}_1')$
242(1)	265(2)[46]	251(4)[9]	A', $[(\delta(\text{F}_5\text{Xe}_1\text{F}_8) + \delta(\text{F}_6\text{Xe}_1\text{F}_7)) - (\delta(\text{F}_5'\text{Xe}_1'\text{F}_8) + \delta(\text{F}_6'\text{Xe}_1'\text{F}_7'))] + \rho_{\text{w}}(\text{F}_1\text{OsF}_2)$
	239(<0.1)[<1]	241(<1)[9]	A'', $\text{Xe}_2\text{F}_{11}^{+}$ def.
	237(2)[1]	237(1)[2]	A', $\delta(\text{F}_1\text{OsF}_1') - \delta(\text{O}_2\text{OsF}_2) + \rho_{\text{t}}(\text{F}_5\text{Xe}_1\text{F}_6) + \rho_{\text{w}}(\text{F}_5'\text{Xe}_1'\text{F}_6') + \delta(\text{Xe}_1\text{F}_3\text{Xe}_1')$
	224(1)[<1]	224(1)[16]	A', $\delta(\text{O}_2\text{OsF}_2) - \delta(\text{F}_1\text{OsF}_1') + \delta(\text{F}_6\text{Xe}_1\text{F}_7) + \delta(\text{F}_6'\text{Xe}_1'\text{F}_7') + \delta(\text{Xe}_1\text{F}_3\text{Xe}_1')$
	212(<0.1)[2]	216(<1)[7]	A'', $\text{Xe}_2\text{F}_{11}^{+}$ def.
203(1)	205(<1)[1]	202(1)[15]	A'', $[\text{Xe}_2\text{F}_{11}][\text{OsO}_3\text{F}_3]$ def.
	196(1)[3]	197(<0.1)[<1]	A', $[\delta(\text{F}_5\text{Xe}_1\text{F}_6) + \delta(\text{F}_5'\text{Xe}_1'\text{F}_6')] - [\delta(\text{F}_7\text{Xe}_1\text{F}_8) + \delta(\text{F}_7'\text{Xe}_1'\text{F}_8')] + [\rho_{\text{w}}(\text{F}_3\text{Xe}_1\text{F}_4) + \rho_{\text{w}}(\text{F}_3\text{Xe}_1'\text{F}_4')]$
	176(<1)[1]	194(<1)[<0.1]	A'', $[\rho_{\text{w}}(\text{F}_4\text{Xe}_1\text{F}_6) + \rho_{\text{t}}(\text{F}_5\text{Xe}_1\text{F}_7)] - [\rho_{\text{w}}(\text{F}_4'\text{Xe}_1'\text{F}_6') + \rho_{\text{t}}(\text{F}_5'\text{Xe}_1'\text{F}_7')]$
	153(<1)[<1]	171(<0.1)[<1]	A'', $[\text{Xe}_2\text{F}_{11}][\text{OsO}_3\text{F}_3]$ def.
167(1)	153(2)[1]	170(<1)[1]	A', $\rho_{\text{w}}(\text{F}_6\text{Xe}_1\text{F}_8) - \rho_{\text{w}}(\text{F}_6'\text{Xe}_1'\text{F}_8') + \delta(\text{F}_3\text{Xe}_1\text{F}_7) - \delta(\text{F}_3\text{Xe}_1'\text{F}_7')$
	167(1)[1]	147(2)[1]	A', $\text{Xe}_2\text{F}_{11}^{+}$ def.
135(1)	133(<1)[1]	134(1)[12]	A', $[\text{Xe}_2\text{F}_{11}][\text{OsO}_3\text{F}_3]$ breathing
	124(<1)[4]	115(1)[5]	$\left\{ \begin{array}{l} \text{A', } [\text{Xe}_2\text{F}_{11}][\text{OsO}_3\text{F}_3] \text{ def.} \\ \text{A', } [\rho_{\text{w}}(\text{F}_4\text{Xe}_1\text{F}_6) + \rho_{\text{t}}(\text{F}_5\text{Xe}_1\text{F}_7)] - [\rho_{\text{w}}(\text{F}_4'\text{Xe}_1'\text{F}_6') + \rho_{\text{t}}(\text{F}_5'\text{Xe}_1'\text{F}_7')] \\ \text{A'', } [\text{Xe}_2\text{F}_{11}][\text{OsO}_3\text{F}_3] \text{ def.} \\ \text{A', } \rho_{\text{w}}(\text{F}_6\text{Xe}_1\text{F}_8) - \rho_{\text{w}}(\text{F}_6'\text{Xe}_1'\text{F}_8') + \delta(\text{F}_3\text{Xe}_1\text{F}_7) - \delta(\text{F}_3\text{Xe}_1'\text{F}_7') \\ \text{A', } \text{Xe}_2\text{F}_{11}^{+} \text{ def.} \\ \text{A', } [\text{Xe}_2\text{F}_{11}][\text{OsO}_3\text{F}_3] \text{ breathing} \end{array} \right.$
110(4)	124(1)[1]	100(1)[1]	
	104(<1)[<1]	97(1)[<0.1]	
	111(<1)[<0.1]	91(1)[1]	
	112(<1)[<0.1]	73(<1)[1]	
	89(<1)[<1]	66(<1)[<1]	
	45(<0.1)[<0.1]	60(<1)[<1]	
	25(<1)[<0.1]	44(<0.1)[<1]	
	96(<1)[<1]	34(<0.1)[<0.1]	
	77(1)[<0.1]	30(1)[<1]	
	63(<0.1)[<0.1]	15(<0.1)[<0.1]	

^a The Raman spectrum was recorded on a microcrystalline sample in a FEP sample tube at -150°C using 1064-nm excitation. Experimental Raman intensities are given in parentheses and are relative intensities with the most intense band given as 100. The abbreviations denote shoulder (sh). A band was also observed at $523(6)\text{ cm}^{-1}$ but was not assigned. ^b Values in parentheses denote calculated Raman intensities ($\text{\AA}^4\text{ u}^{-1}$) and values in square brackets denote calculated infrared intensities (km mol^{-1}). ^c SVWN/SDDall(-PP). ^d B3LYP/ Stuttgart (Os) aug-cc-pVTZ(-PP) (Xe, O, F). ^e Assignments are for the energy-minimized geometry calculated at the B3LYP level of theory. See Figure 7c for the atom labeling scheme. The symbols denote stretch (ν), bend (δ), twist (ρ_{t}), rock (ρ_{r}), wag (ρ_{w}), umbrella (δ_{umb}), and F_5 , F_6 , F_7 , F_8 ($\text{F}_{4\text{e}}$). The abbreviation, def., denotes a deformation mode. ^f The band overlaps with a FEP sample tube band; the intensity is not corrected.

associated with the secondary bonding interactions between the cation and the anion, and are assigned to the coupled $\delta(\text{F}_1\text{OsF}_2) + \delta(\text{F}_3\text{OsO}_3) + \nu(\text{Xe}\cdots\text{F}_3)$ and the $\nu(\text{Xe}\cdots\text{F}_1) + \nu(\text{Xe}\cdots\text{F}_2) + \nu(\text{Xe}\cdots\text{F}_3)$ modes, respectively.

(c) $\text{Xe}_2\text{F}_{11}^{+}$. The vibrational modes of $\text{Xe}_2\text{F}_{11}^{+}$ have not been assigned in detail in prior vibrational studies, e.g., the AsF_6^{-} ,³⁵ PF_6^{-} ,³⁵ PbF_6^{2-} ,³⁷ PdF_6^{2-} ,³⁷ SnF_6^{-} ,³⁷

and VF_6^{-38} salts. The present assignments provide a more detailed description of the vibrational modes of $\text{Xe}_2\text{F}_{11}^{+}$ under C_s symmetry (Table 6).

Among the most noteworthy features of the $\text{Xe}_2\text{F}_{11}^{+}$ Raman spectrum of $[\text{Xe}_2\text{F}_{11}][\text{OsO}_3\text{F}_3]$ are the Xe–F stretching frequencies which occur between 580 and 656 cm^{-1} , and are comparable with other $\text{Xe}_2\text{F}_{11}^{+}$ salts. The band at 591 cm^{-1} is assigned to extensively

coupled Xe–F and Os–F stretches involving the three facial Os–F bond stretches and the 10 primary Xe–F bond stretches of the XeF_5 -units (Table 6). The most intense Xe–F stretching band at 656 cm^{-1} is assigned to the $[\nu(\text{Xe}_1\text{F}_4) + \nu(\text{Xe}_1\text{F}_5) + \nu(\text{Xe}_1\text{F}_6)] + [\nu(\text{Xe}_1'\text{F}_4') + \nu(\text{Xe}_1'\text{F}_5') + \nu(\text{Xe}_1'\text{F}_6')]$ stretching mode and is in good agreement with the most intense cation band of other $\text{Xe}_2\text{F}_{11}^+$ salts, e.g., AsF_6^- (663 cm^{-1}),³⁵ PF_6^- (666 cm^{-1}),³⁵ PbF_6^{2-} (650 cm^{-1}),³⁷ PdF_6^{2-} (651 cm^{-1}),³⁷ SnF_6^{2-} (657 cm^{-1}),³⁷ and VF_6^- (655 cm^{-1}).³⁸ The $\text{Xe}_1\cdots\text{F}_3\cdots\text{Xe}_1'$ bridge stretches are predicted to be weak and to occur at 370, 335, and 300 (SVWN) and 329, 322, and 276 (B3LYP) cm^{-1} , but could not be observed. In the present case, the symmetric $\nu(\text{Xe}_1\text{F}_3) + \nu(\text{Xe}_1'\text{F}_3)$ bridge stretch is in-phase coupled to the $\delta_{\text{umb}}(\text{XeF}_{4e}) + \delta_{\text{umb}}(\text{Xe}_1'\text{F}_{4e'})$ bending mode, whereas the asymmetric $\nu(\text{Xe}_1\text{F}_3) - \nu(\text{Xe}_1'\text{F}_3)$ bridge stretch is in-phase coupled to both the $\rho_t(\text{F}_1\text{OsF}_1') + \rho_w(\text{F}_2\text{OsO}_2)$ and the $\rho_t(\text{O}_1\text{OsO}_1') - \rho_t(\text{F}_1\text{OsF}_1')$ bending modes. The three modes are predicted to occur between 300 and 370 (SVWN) and 276–329 (B3LYP) cm^{-1} .

Computational Results. The structures of $[\text{XeF}_5]^-$, $[\mu\text{-F}(\text{OsO}_3\text{F}_2)_2]$ (C_{2v}), $[\text{XeF}_5][\text{OsO}_3\text{F}_3]$ (C_s), $[\text{Xe}_2\text{F}_{11}]^+$, $[\text{OsO}_3\text{F}_3]^-$ (C_s), XeF_5^+ (C_{4v}), $\text{Xe}_2\text{F}_{11}^+$ (C_s), OsO_3F_3^- (C_{3v}), and $\mu\text{-F}(\text{OsO}_3\text{F}_2)_2^-$ (C_2) (Figure 7 and Figures S5 and S6 in the Supporting Information) were optimized using SVWN and B3LYP methods under the specified symmetries and resulted in stationary points with all frequencies real. The geometrical parameters and vibrational frequencies were benchmarked, as previously described, using *cis*- OsO_2F_4 and XeOF_4 .⁵

(a) Calculated Geometries. The calculated ion-pair geometries of $[\text{XeF}_5][\mu\text{-F}(\text{OsO}_3\text{F}_2)_2]$ (Table 2), $[\text{XeF}_5][\text{OsO}_3\text{F}_3]$, and $[\text{Xe}_2\text{F}_{11}][\text{OsO}_3\text{F}_3]$ (Table 3) are in good agreement with the experimental geometries, with slightly better agreement for the Xe–F bond lengths at the B3LYP level, and for the Os–F and Os–O bond lengths of the $[\text{XeF}_5][\text{OsO}_3\text{F}_3]$ and $[\text{Xe}_2\text{F}_{11}][\text{OsO}_3\text{F}_3]$ salts at the SVWN level. The calculations confirm that the gas-phase ion pairs are stable entities, and all trends in their crystal structures are reproduced by the calculated ion-pair geometries, with the largest discrepancies occurring for the $\text{Xe}\cdots\text{F}$ contact distances. In all cases, the SVWN calculations predict slightly shorter secondary bonding interactions than the B3LYP calculations (Tables 2 and 3).

The calculated geometries of the $[\text{XeF}_5][\mu\text{-F}(\text{OsO}_3\text{F}_2)_2]$ and $[\text{XeF}_5][\text{OsO}_3\text{F}_3]$ ion pairs are in better agreement with their experimental geometries than $[\text{Xe}_2\text{F}_{11}][\text{OsO}_3\text{F}_3]$, underscoring that both ion pairs are well isolated in their crystal structures, showing no inter-ion pair contacts. The experimental $\text{Os}\cdots\text{F}_3\cdots\text{Os}'$ bridge bond lengths of $[\text{XeF}_5][\mu\text{-F}(\text{OsO}_3\text{F}_2)_2]$ (2.1179(5) Å) are particularly well modeled by both the B3LYP (2.147 Å) and SVWN (2.115 Å) structures. The $\text{Os}\cdots\text{F}_3\cdots\text{Os}'$ bridge bond angle (155.5(1)°) is also very well reproduced at the B3LYP (155.4°) and SVWN (150.9°) levels. For this structure, the $\text{Xe}\cdots\text{F}$ contact distances calculated at the B3LYP (2.643 and 2.644 Å) level better reproduce the experimental values (2.622(1) and 2.663(1) Å) than those calculated at the SVWN level (2.461 and 2.461 Å).

The calculated structure of the $[\text{Xe}_2\text{F}_{11}][\text{OsO}_3\text{F}_3]$ ion pair does not take into account the additional $\text{Xe}\cdots\text{O}$

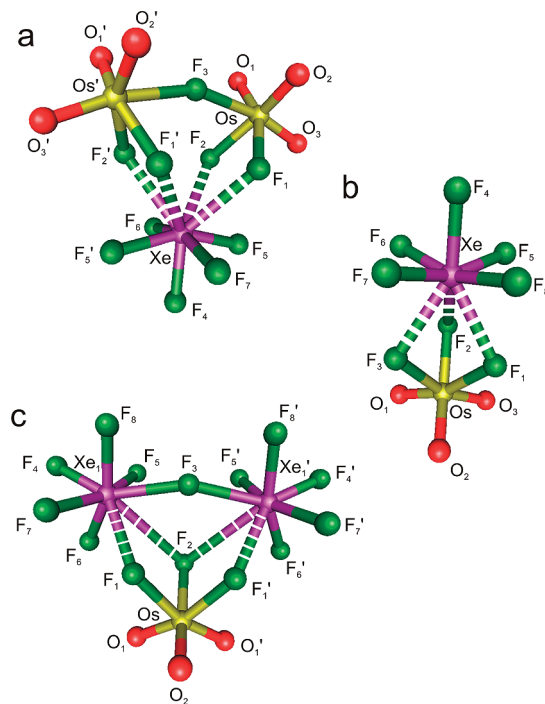


Figure 7. Calculated gas-phase geometries at the B3LYP level of theory for (a) $[\text{XeF}_5][\mu\text{-F}(\text{OsO}_3\text{F}_2)_2]$ (C_{2v}), (b) $[\text{XeF}_5][\text{OsO}_3\text{F}_3]$ (C_s), and (c) $[\text{Xe}_2\text{F}_{11}][\text{OsO}_3\text{F}_3]$ (C_s).

inter-ion pair contact (vide supra) and consequently does not reproduce the experimental ion-pair geometry as well. The tri-coordination of F(2) is reproduced, but the $\text{Xe}_1\cdots\text{F}_2$ and $\text{Xe}_2\cdots\text{F}_2$ contact distances at the B3LYP level (3.197 and 3.197 Å) are significantly longer than the SVWN (2.613 and 2.613 Å) and the experimental (2.800(2) Å) values.

The geometries of the isolated gas-phase cations and anions have also been calculated to assess the effects of ion pairing on the primary bond lengths and angles. The fluorine atoms of the ion-paired OsO_3F_3^- anions strongly coordinate to xenon, elongating the Os–F bonds (av. 2.022, SVWN; 2.031, B3LYP Å) when compared with those of the gas-phase OsO_3F_3^- anion (1.950, SVWN; 1.961, B3LYP Å) (Table S5, Supporting Information). As a result, the Os–O bond lengths of the ion pair are significantly shorter (av. 1.711, SVWN; 1.689, B3LYP Å) than those of the free anion (1.737, SVWN; 1.711, B3LYP Å). The same trends are observed for $\mu\text{-F}(\text{OsO}_3\text{F}_2)_2^-$ (Table 2), that is, the Os–O bond lengths are shortened and the Os–F_{1,2} bond lengths are elongated upon coordination to XeF_5^+ . The $\text{Os}\cdots\text{F}\cdots\text{Os}$ bond angle of the free $\mu\text{-F}(\text{OsO}_3\text{F}_2)_2^-$ anion is more closed (143.0°, SVWN; 140.7°, B3LYP) relative to that of the gas-phase ion pair (150.9°, SVWN; 155.4°, B3LYP) because chelation of the XeF_5^+ cation through xenon contacts with the fluorine ligands of the anion results in compression of this angle. In contrast, the $\text{Xe}\cdots\text{F}\cdots\text{Xe}$ bond angle of the free $\text{Xe}_2\text{F}_{11}^+$ cation is more open (141.8°, SVWN; 171.2°, B3LYP) than in $[\text{Xe}_2\text{F}_{11}][\text{OsO}_3\text{F}_3]$ (129.3°, SVWN; 152.2°, B3LYP), which is again attributed to coordination of the anion fluorine ligands to xenon, leading to compression of the $\text{Xe}\cdots\text{F}\cdots\text{Xe}$ angle in the chelate relative to that of the free $\text{Xe}_2\text{F}_{11}^+$ cation. The Xe–F bond lengths of the free XeF_5^+ (Table 2) and $\text{Xe}_2\text{F}_{11}^+$

(Table S6, Supporting Information) cations are slightly shorter than in their respective ion pairs as a consequence of the extra electron density donated to the xenon cation by the anion, resulting in longer, more polar primary Xe–F bonds in the ion pairs (see below for anion–cation charge drift values).

(b) Charges, Valencies, and Bond Orders. The Natural Bond Orbital (NBO)^{39–42} analyses were carried out for the optimized B3LYP [SVWN] gas-phase geometries of $[\text{XeF}_5][\mu\text{-F}(\text{OsO}_3\text{F}_2)_2]$, $[\text{XeF}_5][\text{OsO}_3\text{F}_3]$, $[\text{Xe}_2\text{F}_{11}][\text{OsO}_3\text{F}_3]$ (Table S7, Supporting Information), XeF_5^+ , $\text{Xe}_2\text{F}_{11}^+$ (Table S8, Supporting Information), OsO_3F_3^- , and $\mu\text{-F}(\text{OsO}_3\text{F}_2)_2^-$ (Table S9, Supporting Information).

The NPA (Natural Population Analysis) gave positive charges of 2.19 [1.88], 2.17 [1.87], and 2.18 [1.87] for osmium and 3.29 [3.05], 3.28 [3.04], and 3.29 [3.06] for xenon in the $[\text{XeF}_5][\mu\text{-F}(\text{OsO}_3\text{F}_2)_2]$, $[\text{XeF}_5][\text{OsO}_3\text{F}_3]$, and $[\text{Xe}_2\text{F}_{11}][\text{OsO}_3\text{F}_3]$ ion pairs, respectively. The negative charges of the light atoms indicate that the bonding in the ion pairs is polar covalent. The average charges of the oxygen ligands are less negative than the average charges of the fluorine ligands in both the anions and the cations, which is consistent with significant charge transfer from the filled oxygen p orbitals into the empty d orbitals of osmium. Overall, the fluorine ligands of the anions are more negative than those of the cations, which is consistent with the net charges of the cation and anion.

The Xe---F₃ bridge bond orders of $[\text{Xe}_2\text{F}_{11}][\text{OsO}_3\text{F}_3]$ (0.18 [0.20]) and the Os---F₃ bond orders of $[\text{XeF}_5][\mu\text{-F}(\text{OsO}_3\text{F}_2)_2]$ (0.21 [0.25]) are significantly less than those of the terminal Xe–F (av. 0.46–0.50 [0.41–0.46]) and Os–F (av. 0.29–0.38 [0.32–0.37]) bonds of either salt because the bridging fluorine atoms are equally shared between the two electropositive heavy atoms. Although the Xe---F₃ and Os---F₃ bridge bond orders are similar, the average terminal Xe–F bond orders of XeF_5^+ and $\text{Xe}_2\text{F}_{11}^+$ are more than double the bridging Xe---F₃ bond order in $\text{Xe}_2\text{F}_{11}^+$. In contrast, the average terminal Os–F bond orders of OsO_3F_3^- and $\mu\text{-F}(\text{OsO}_3\text{F}_2)_2^-$ are less than twice the Os---F₃ bridge bond order. The difference is attributable to significantly higher positive charges on the xenon atoms than on the osmium atoms (Table S7, Supporting Information), which result in lower negative charges on the fluorine atoms of the xenon cations and more covalent Xe–F bonds than for fluorine bonded to osmium.

The Os–O bond orders of both ion pairs are similar (0.87–0.88 [0.86–0.86]) but slightly greater than those of the free anions (0.85–0.86 [0.81–0.83]). The Os–F bond orders (0.29–0.38 [0.32–0.37]) are also similar but less than those of the free anions (0.38–0.41 [0.39–0.42]). Both features result from significant fluorine bridge interactions between the fluorine ligands of osmium and xenon atoms of the ion pairs. The somewhat higher Os–O

bond orders compensate for the negative charge drift onto the cation via the secondary bonding interactions. The calculated negative charge drifts from anion to cation within the ion pair reflect this trend: $[\text{XeF}_5][\mu\text{-F}(\text{OsO}_3\text{F}_2)_2]$, 0.19 [0.37]; $[\text{XeF}_5][\text{OsO}_3\text{F}_3]$, 0.25 [0.39]; $[\text{Xe}_2\text{F}_{11}][\text{OsO}_3\text{F}_3]$, 0.23 [0.37].

Other than the Xe---F₃ bridge bond orders of $\text{Xe}_2\text{F}_{11}^+$, the secondary Xe...F bond orders range from 0.02 [0.10] for the F₂ atom of $[\text{Xe}_2\text{F}_{11}][\text{OsO}_3\text{F}_3]$ to 0.12 [0.16] for the F₁ and F₃ atoms of $[\text{XeF}_5][\text{OsO}_3\text{F}_3]$. The lower Xe...F₂ bond order results from the interaction of F₂ with both xenon atoms of the $\text{Xe}_2\text{F}_{11}^+$ cation. The higher Xe...F_{1,3} bond orders of $[\text{XeF}_5][\text{OsO}_3\text{F}_3]$ when compared with the Xe...F_{1,2} bond orders of $[\text{XeF}_5][\mu\text{-F}(\text{OsO}_3\text{F}_2)_2]$ correlate with the higher positive charge on xenon that results from only eight primary and secondary contacts to xenon instead of nine as in the remaining two ion pairs (see Calculated Geometries).

The axial and equatorial Xe–F bond orders of XeF_5^+ and $\text{Xe}_2\text{F}_{11}^+$ are only slightly altered upon coordination of either cation to OsO_3F_3^- . The equatorial Xe–F bond orders for all three ion pairs are similar (0.47–0.48 [0.41–0.44]) and are only slightly less than those of free XeF_5^+ and $\text{Xe}_2\text{F}_{11}^+$ (0.48–0.49 [0.48]). The axial Xe–F bonds of the ion pairs have significantly higher bond orders (0.50 [0.45–0.46]) than the equatorial Xe–F bonds. The axial Xe–F bond orders of the ion pairs are similar to those of the free cations calculated at the B3LYP level (0.51–0.53), but at the SVWN level they are somewhat higher for the free cations (0.50–0.52). The lower Xe–F bond orders for all of the ion pairs relative to those of free XeF_5^+ and $\text{Xe}_2\text{F}_{11}^+$ are in accord with the calculated anion–cation charge drifts (vide supra).

Conclusions

The $[\text{XeF}_5][\mu\text{-F}(\text{OsO}_3\text{F}_2)_2]$, $[\text{XeF}_5][\text{OsO}_3\text{F}_3]$, and $[\text{Xe}_2\text{F}_{11}][\text{OsO}_3\text{F}_3]$ salts have been synthesized by the reactions of stoichiometric mixtures of XeF_6 and $(\text{OsO}_3\text{F}_2)_\infty$. All three salts are room-temperature stable but dissociate back to the starting materials after prolonged heating at 50 °C. The salts provide the only examples of noble-gas cations that are stabilized by metal oxide fluoride anions and the first example of a salt of the fluorine-bridged $\mu\text{-F}(\text{OsO}_3\text{F}_2)_2^-$ anion. All three salts exist as discrete ion pairs in which the fluorine ligands of the osmium oxide fluoride anions mainly interact by means of secondary bonding interactions with the xenon atoms of the cations. Ion-pairing results in nine-coordination at the xenon atoms of $[\text{XeF}_5][\mu\text{-F}(\text{OsO}_3\text{F}_2)_2]$ and $[\text{Xe}_2\text{F}_{11}][\text{OsO}_3\text{F}_3]$ and eight-coordination at the xenon atom of $[\text{XeF}_5][\text{OsO}_3\text{F}_3]$. The primary coordination spheres of the osmium atoms of $\mu\text{-F}(\text{OsO}_3\text{F}_2)_2^-$ and OsO_3F_3^- are pseudo-octahedral with facial arrangements of oxygen and fluorine ligands. The OsO_3F_3^- anions have geometrical parameters that are closer to those of neutral trioxo Os(VIII) species, indicating that the XeF_5^+ and $\text{Xe}_2\text{F}_{11}^+$ cations withdraw significant electron density from the anion by means of their secondary bonding interactions. Quantum-chemical calculations have been used to model the ion pairs and their component ions and provide energy-minimized geometries that are in very good agreement with the experimental structures. The Raman spectra of all three salts have been fully assigned based on the calculated vibrational modes.

(39) Reed, A. E.; Weinstock, R. B.; Weinhold, F. *J. Chem. Phys.* **1985**, *83*, 735–746.

(40) Glendening, E. D.; Reed, A. E.; Carpenter, J. E.; Weinhold, F. *NBO*, Version 3.1; Gaussian Inc.: Pittsburgh, PA, 1990.

(41) Reed, A. E.; Curtiss, L. A.; Weinhold, F. *Chem. Rev.* **1998**, *88*, 899–926.

(42) Glendening, E. D.; Badenhoop, J. K.; Reed, A. E.; Carpenter, J. E.; Bohmann, C. M.; Morales, C. M.; Weinhold, F. *NBO*, Version 5.0; Theoretical Chemical Institute, University of Wisconsin: Madison, WI, 2001.

Experimental Section

Apparatus and Materials. Manipulations involving air-sensitive materials were carried out under anhydrous conditions as previously described.⁴³ All preparative work was carried out in FEP reaction vessels fabricated from 1/4-in. o.d. lengths of tubing, unless otherwise noted, that had been heat-sealed at one end and connected by means of 45° SAE flares and compression fittings to Kel-F valves. Reaction vessels were dried on a Pyrex glass vacuum line and then transferred to a metal vacuum line where they were passivated with F₂ for several hours, refilled with dry N₂, and placed in a drybox until used. All vacuum line connections were made by use of 1/4-in. 316 stainless steel Swagelok Ultratorr unions fitted with Viton O-rings. Osmium trioxide difluoride, (OsO₃F₂)_∞, was synthesized by reaction of OsO₄ (Koch-Light, 99.9%) with ClF₃.¹² Xenon hexafluoride, XeF₆, was synthesized by reaction of xenon gas with elemental fluorine,⁴⁴ and XeOF₄ was synthesized by hydrolysis of XeF₆.⁴⁵ Commercial anhydrous HF (Harshaw Chemicals Co.) was further dried by treatment with elemental fluorine using the standard literature procedure.⁴⁶

Synthesis of [XeF₅][μ-F(OsO₃F₂)₂]. On a metal vacuum line, 0.0296 g (0.121 mmol) of XeF₆ was sublimed into a 1/4-in. o.d. FEP weighing vessel. Inside the drybox, a 4-mm FEP reaction tube was loaded with 0.0496 g (0.180 mmol) of orange (OsO₃F₂)_∞. The reaction vessel and weighing vessel were then transferred to a metal vacuum line, and XeF₆ (0.0228 g, 0.0930 mmol) was sublimed from the weighing vessel into the reaction vessel containing (OsO₃F₂)_∞ under static vacuum at −196 °C. Warming the reaction mixture to room temperature (25 °C) initially resulted in a deep orange liquid and unreacted (OsO₃F₂)_∞. The sample solidified, as (OsO₃F₂)_∞ was consumed, to form orange crystalline [XeF₅][μ-F(OsO₃F₂)₂]. Heating the sample at 50 °C for 1 h under 1 atm of dry N₂ to ensure complete reaction did not result in any physical changes.

Synthesis of [XeF₅][OsO₃F₃]. Following a synthetic procedure similar to that outlined for [XeF₅][μ-F(OsO₃F₂)₂], 0.0772 g (0.315 mmol) of XeF₆ was initially sublimed into a FEP weighing vessel and 0.0675 g (0.244 mmol) of (OsO₃F₂)_∞ was loaded into a FEP reaction vessel. Xenon hexafluoride (0.0614 g, 0.250 mmol) was sublimed from the weighing vessel into the reaction vessel containing (OsO₃F₂)_∞. Upon warming to room temperature (25 °C), a deep orange liquid formed. The sample was heated at 50 °C for 1 h under 1 atm of dry N₂ to ensure complete reaction, and upon cooling to 0 °C, an orange crystalline solid formed.

Synthesis of [Xe₂F₁₁][OsO₃F₃]. Following a synthetic procedure similar to that outlined for [XeF₅][μ-F(OsO₃F₂)₂], 0.1255 g (0.512 mmol) of XeF₆ was initially sublimed into a FEP weighing vessel and 0.0601 g (0.218 mmol) of orange (OsO₃F₂)_∞ was loaded into a FEP reaction vessel. Xenon hexafluoride, 0.1224 g (0.499 mmol) was sublimed from the weighing vessel into the reaction vessel containing (OsO₃F₂)_∞. Upon warming the reaction mixture to room temperature (25 °C), a light orange crystalline solid formed. The sample was then warmed to 50 °C under 1 atm of dry N₂, whereupon the sample melted, forming a deep orange liquid which solidified upon cooling to room temperature.

Note: prolonged heating (> 2 h) of all three salts to 50 °C under 1 atm of nitrogen led to sublimation of XeF₆ out of the heated zone and condensation on the cooler walls of the reaction vessel.

Raman Spectroscopy. The low-temperature Raman spectra of [XeF₅][μ-F(OsO₃F₂)₂], [XeF₅][OsO₃F₃], and [Xe₂F₁₁][OsO₃F₃], (−150 °C) were recorded on a Bruker RFS 100 FT Raman spectrometer using 1064-nm excitation and a resolution of 1 cm^{−1} as previously described.⁴ The spectra were recorded using a laser power of 300 mW and a total of 1500, 900, and 1200 scans, respectively.

X-ray Crystallography. (a) Crystal Growing. Details of crystal growing are provided in the Supporting Information. Crystals of [XeF₅][μ-F(OsO₃F₂)₂], [XeF₅][OsO₃F₃], and [Xe₂F₁₁][OsO₃F₃] having the dimensions 0.39 × 0.10 × 0.10, 0.21 × 0.21 × 0.20, and 0.39 × 0.11 × 0.07 mm³, respectively, were selected at −105 ± 3 °C for low-temperature X-ray structure determination and were mounted in a cold stream (−173 °C) on a goniometer head as previously described.⁴

(b) Collection and Reduction of X-ray Data. Crystals were centered on a Bruker SMART APEX II diffractometer, equipped with an APEX II 4K CCD area detector and a triple-axis goniometer, controlled by the APEX2 Graphical User Interface (GUI) software,⁴⁷ and a sealed source emitting graphite-monochromated Mo-Kα radiation (λ = 0.71073 Å). Diffraction data collection at −173 °C consisted of a full ϕ-rotation at a fixed χ = 54.74° with 0.36° (1010) frames, followed by a series of short (250 frames) ω scans at various ϕ settings to fill the gaps. The crystal-to-detector distances were 4.976, 4.954, and 4.969 cm for [XeF₅][μ-F(OsO₃F₂)₂], [XeF₅][OsO₃F₃], and [Xe₂F₁₁][OsO₃F₃], respectively, and the data collections were carried out in a 512 × 512 pixel mode using 2 × 2 pixel binning. Processing of the raw data sets were completed by using the APEX2 GUI software,⁴⁷ which applied Lorentz and polarization corrections to three-dimensionally integrated diffraction spots. The program SADABS,⁴⁸ was used for the scaling of diffraction data, the application of decay corrections, and empirical absorption corrections on the basis of the intensity ratios of redundant reflections.

(c) Solution and Refinement of the Structures. The XPREP⁴⁹ program was used to confirm the unit cell dimensions and the crystal lattices. The solution was obtained by direct methods which located the positions of the atoms defining [XeF₅]-[μ-F(OsO₃F₂)₂], [XeF₅][OsO₃F₃], and [Xe₂F₁₁][OsO₃F₃]. The final refinement was obtained by introducing anisotropic thermal parameters and the recommended weightings for all of the atoms. The maximum electron densities in the final difference Fourier maps were located near the heavy atoms. All calculations were performed using the SHELXTL-plus package⁴⁹ for the structure determinations and solution refinements and for the molecular graphics. The choices of space group for [XeF₅]-[μ-F(OsO₃F₂)₂], [XeF₅][OsO₃F₃], and [Xe₂F₁₁][OsO₃F₃] were confirmed by Platon from the WinGX software package.⁵⁰

Computational Methods

The optimized geometries and frequencies of the ion pairs [XeF₅][μ-F(OsO₃F₂)₂], [XeF₅][OsO₃F₃], [Xe₂F₁₁][OsO₃F₃] and of the ions XeF₅⁺, Xe₂F₁₁⁺, OsO₃F₃[−], and μ-F(OsO₃F₂)₂[−] were calculated at the SVWN and B3LYP⁵¹ levels of theory. The Stuttgart semi-relativistic large core and effective core pseudopotential basis sets (SDDall) augmented for F, O, and Xe with two d-type polarization functions by Huzinaga⁵² were

(47) APEX2, Release 2.0-2; Bruker AXS Inc.: Madison, WI, 2005.

(48) Sheldrick, G. M. *SADABS (Siemens Area Detector Absorption Corrections)*, version 2.10; Siemens Analytical X-ray Instruments Inc.: Madison, WI, 2004.

(49) Sheldrick, G. M. *SHELXTL-Plus*, release 6.14; Siemens Analytical X-ray Instruments, Inc.: Madison, WI, 2000–2003.

(50) Farrugia, L. J. *J. Appl. Crystallogr.* **1999**, *32*, 837–838.

(51) Frisch, M. J. et. *Gaussian 03*, Revision B.04; Gaussian, Inc.: Pittsburgh, PA, 2003.

(52) Huzinaga, S.; Andzelm, J.; Kolobukowski, M.; Radzio-Andzelm, E.; Sakai, Y.; Tatewaki, H. *Gaussian Basis Sets for Molecular Calculations*; Physical Science Data 16; Elsevier: Amsterdam, The Netherlands, 1984.

(43) Casteel, W. J.; Dixon, D. A.; Mercier, H. P. A.; Schrobilgen, G. J. *Inorg. Chem.* **1996**, *35*, 4310–4322.

(44) Chernick, C. L.; Malm, J. G. *Inorg. Synth.* **1966**, *8*, 259–260.

(45) Schumacher, G. A.; Schrobilgen, G. J. *Inorg. Chem.* **1984**, *23*, 2923–2929.

(46) Emara, A. A. A.; Schrobilgen, G. J. *Inorg. Chem.* **1992**, *31*, 1323–1332.

used at the SVWN level, and the Stuttgart basis set augmented by one f-type polarization function (α_f Os 0.886)⁵³ for osmium and aug-cc-pVTZ basis sets for xenon, oxygen, and fluorine were used at the B3LYP level.

Pseudopotentials were used with the appropriate basis sets for both osmium (SDDall-PP) and xenon (aug-cc-pVTZ-PP). The combined use of SDDall and SDDall-PP or aug-cc-pVTZ and aug-cc-pVTZ-PP basis sets are indicated as SDDall(-PP) or aug-cc-pVTZ(-PP). Quantum-chemical calculations were carried out using the program Gaussian 03.⁵¹ The levels and basis sets were benchmarked by calculating *cis*-OsO₂F₄ and XeOF₄ as previously described.⁵ The geometries were fully optimized using analytical gradient methods. After optimization at one level of theory, the geometries were calculated at the other level of theory to ensure an equivalent energy-minimized geometry had been achieved. The vibrational frequencies were calculated at the SVWN and B3LYP levels using the appropriate minimized structure, and the vibrational mode descriptions were arrived at with the aid of Gaussview.⁵⁴

Acknowledgment. We thank the Natural Sciences and Engineering Research Council of Canada for the award of post-graduate scholarships (M.J.H.) and for support in the form of a Discovery Grant (G.J.S.). The computations were conducted with the aid of the facilities of the Shared Hierarchical

Academic Research Computing Network. (SHARCNET: www.Sharcnet.ca.)

Supporting Information Available: Comprehensive lists of known XeF₅⁺ and Xe₂F₁₁⁺ salts and their references; discussion of the crystal packing in [XeF₅][μ -F(OsO₃F₂)₂], [XeF₅][OsO₃F₃], and [Xe₂F₁₁][OsO₃F₃]; view of the crystallographic unit cell along the *c*-axis for [XeF₅][μ -F(OsO₃F₂)₂] (Figure S1), [XeF₅][OsO₃F₃] (Figure S2), and [Xe₂F₁₁][OsO₃F₃] (Figure S3); the primary coordination sphere formed by the light atoms of the OsO₃F₃-unit (Figure S4); interatomic distances between the light atoms forming the coordination spheres of the Xe and Os atoms in [XeF₅][μ -F(OsO₃F₂)₂], [XeF₅][OsO₃F₃], and [Xe₂F₁₁][OsO₃F₃] (Table S1); factor-group analyses for [XeF₅][μ -F(OsO₃F₂)₂] (Table S2), [XeF₅][OsO₃F₃] (Table S3), and [Xe₂F₁₁][OsO₃F₃] (Table S4); discussion of factor-group analyses for [XeF₅][μ -F(OsO₃F₂)₂], [Xe₂F₁₁][OsO₃F₃], and [Xe₂F₁₁][OsO₃F₃]; calculated B3LYP gas-phase geometries for XeF₅⁺ and Xe₂F₁₁⁺ (Figure S5) and for OsO₃F₃⁻ and μ -F(OsO₃F₂)₂⁻ (Figure S6); calculated geometrical parameters for OsO₃F₃⁻ (*C*_{3v}) (Table S5) and Xe₂F₁₁⁺ (*C*_s) (Table S6); natural bond orbital (NBO) valencies, bond orders and NPA charges for [XeF₅][μ -F(OsO₃F₂)₂], [XeF₅][OsO₃F₃], and [Xe₂F₁₁][OsO₃F₃] (Table S7), for XeF₅⁺ and Xe₂F₁₁⁺ (Table S8), and for OsO₃F₃⁻ and μ -F(OsO₃F₂)₂⁻ (Table S9); details of crystal growing for [XeF₅][μ -F(OsO₃F₂)₂], [XeF₅][OsO₃F₃], and [Xe₂F₁₁][OsO₃F₃]; complete reference 51; The X-ray crystallographic files in CIF format for the structure determination of [XeF₅][μ -F(OsO₃F₂)₂], [XeF₅][OsO₃F₃], and [Xe₂F₁₁][OsO₃F₃]. This material is available free of charge via the Internet at <http://pubs.acs.org>.

(53) Ehlers, A. W.; Bohme, M.; Dapprich, S.; Gobbi, A.; Hollwarth, A.; Jonas, V.; Kohler, K. F.; Stegmann, R.; Veldkamp, A.; Frenking, G. *Chem. Phys. Lett.* **1993**, *208*, 111–114.

(54) *GaussView*, release 3.0; Gaussian Inc.: Pittsburgh, PA, 2003.